



TAMPERE UNIVERSITY OF TECHNOLOGY

SEYED KOUROSH LATIFI

MEASUREMENT OF Z-DIRECTIONAL INDIVIDUAL FIBRE-FIBRE  
BOND STRENGTH AND MICROFIBRIL ANGLE USING  
MICROROBOTICS

Master of Science Thesis

Examiner: Professor Pasi Kallio  
Examiner and topic approved by the  
Council of the Faculty of  
Engineering Sciences on  
05.11.2014.

## ABSTRACT

TAMPERE UNIVERSITY OF TECHNOLOGY

Master's Degree Programme in Machine Automation

**LATIFI, SEYED KOUROSH:** Measurement of Z-Directional Individual Fibre-Fibre Bond Strength and Microfibril Angle Using Microrobotics

Master of Science Thesis, 71 pages, 0 Appendix pages

November 2014

Major: Mechatronics and Micromachines

Examiner: Professor Pasi Kallio

Keywords: Microrobotics, Microforce Sensing, Polyvinylidene fluoride (PVDF), Transmission Ellipsometry, Z-Directional Strength, Microfibril angle.

The use of microrobotics in high throughput and precise characterization of objects at microscale has been noticeably increased during recent years. Microrobotics has provided a significant added value to multiple realms e.g. biomedical research, bio-based industry, microassembly of miniature products, etc. Recently, the use of microrobotic technology in paper industry has been also commenced for measuring properties at the single fibre level.

There is a large interest in the measurement of different loading modes of individual fibre-fibre bonds in pulp and paper/board industry. Among the four different modes of loading, it would be desirable for papermaking companies and paper converting companies to obtain the Z-directional strength of pulp and paper. Indeed, the Z-directional properties affect compressive properties, and accordingly the performance of structural paperboard products. Several methods have been developed to measure the Z-directional strength at a handsheet level; however, there is not any reported device capable of the Z-directional fibre-fibre bond strength measurement at a fibre level. This thesis work presents a novel method for the experimental evaluation of the Z-directional bond strength using microrobotics and a Polyvinylidene fluoride (PVDF) film microforce sensor. Due to the special dynamics of PVDF microforce sensors, the effect of the deformation rate on the performance of the sensor is studied. The Z-directional fibre-fibre bond strength experiments have been performed successfully for unrefined and refined bleached softwood Kraft pulp fibres.

Besides, paper scientists are interested in microfibril angle changes during and after application of the Z-directional force. Indeed, there is interest in simultaneous measurement of microfibril angle and mechanical properties such as Z-directional bond strength. To address this need, a microfibril angle measurements system based on microscopic transmission ellipsometry is developed and integrated to the microrobotic platform. The results from both Z-directional bond strength and microfibril angle measurement are promising.

In summary, the first concept for simultaneous measurement of microfibril angle and mechanical properties such as Z-directional bond strength at the individual fibre level is developed during this thesis work which has a high practical impact on the fibre characterization research field.

## PREFACE

This thesis work was accomplished in the Micro- and Nanosystems Research Group of the Department of Automation Science and Engineering at Tampere University of Technology. I would like to acknowledge the Academy of Finland for supporting this work by funding PowerBonds (Grant No.:256527) and Fibam (Grant No.: 253364) projects.

I owe my deepest gratitude to my supervisor Prof. Pasi Kallio for guidance, support, inspiring collaboration, and for providing the didactical background on which this work is based.

My warm thanks go to Pooya Saketi for his constructive collaboration which improved the quality of this thesis and also his helps in hardware development of the microrobotic platform. My thanks are extended to several colleagues at the department of Automation Science and Engineering. Among the many, I wish to mention Juha Hirvonen and Mathias von Essen in our Research Group for developing the vision system, and the software and user interface of the platform, respectively.

My heartfelt gratitude goes to my wife Parvin who taught me how to love. She has been a great overseas spiritual support during my studies in Finland. Without her support, this work would never have been completed, and all of my achievements belong to her. I would like to also extend my appreciation and respect to my mother and brother who have been a great source of encouragement.

Finally, I would like to thank all of my friends and beloved ones in Finland specially Hamed, Beheshteh, Peyman, Mohammad, and Arash for giving me beautiful unlimited memories that I am going to cherish for a lifetime.

Tampere, November 2014  
SEYED KOUROSH LATIFI

## TABLE OF CONTENTS

List of figures .....	V
List of tables .....	VIII
List of abbreviations .....	IX
List of symbols .....	X
1. Introduction.....	1
1.1. Problem Statement .....	2
1.2. Research Objectives and Expected Results .....	3
1.3. Research Method Explanation .....	4
1.4. Overview of the PowerBonds Project .....	4
1.5 Collaboration.....	5
1.6. Thesis Outline .....	5
2. Theoretical Background and Framework .....	7
2.1. Microrobotic Manipulation Systems .....	7
2.1.1. Components of Microrobotic Manipulation Systems.....	8
2.1.2. Applications of Microrobotic Manipulation Systems.....	9
2.2. Piezoelectric Effect.....	10
2.3. Microforce Sensing .....	11
2.3.1. Strain Gauge .....	12
2.3.2. Piezoelectric Force Sensor .....	13
2.3.3. Capacitive Force Sensor .....	15
2.3.4. Optical Force Sensor.....	16
2.4. Paper Fibre Properties .....	17
2.4.1. Z-Directional Individual Fibre-Fibre Bond Strength.....	19
2.4.2. Microfibril Angle.....	21
2.5. Existing Functionalities of TUT's Microrobotic Platform for Fibre Characterization .....	26
2.6. T-test Analysis .....	28
2.7. Discussion .....	30
3. Research Methods and Materials .....	32

3.1. Overview of the Microrobotic Platforms.....	32
3.2. Z-Directional Individual Fibre-Fibre Bond Strength Measurement Method...	35
3.2.1. Conceptual Design.....	35
3.2.2. Microforce Sensing System Design and Implementation.....	37
3.2.3. Microforce Sensing System Calibration .....	40
3.2.4. Individual Fibre-Fibre Bond Making.....	45
3.2.5. Z-Directional Bond Strength Measurement Protocol.....	46
3.3. Microfibril Angle Measurement Method.....	48
3.3.1. Conceptual Design.....	48
3.3.2. Hardware Design and Implementation .....	50
3.4. Discussion.....	52
4. Results and Discussion.....	53
4.1. Effect of Deformation Rate on Microforce Sensor Response .....	53
4.2. Z-Directional Fibre-Fibre Bond Strength Measurement Results .....	55
4.2.1. The Effect of Refining on Z-Directional Bond Strength .....	55
4.2.2. T-Test Analysis of the Results .....	57
4.3. Microfibril Angle Measurement - Performance Experiments .....	57
4.4. Discussion.....	62
5. Conclusions.....	64
References .....	66

## LIST OF FIGURES

Figure 2.1 - Examples of micro-mechanisms: micro-gear (left); micro-motor (right).....	9
Figure 2.2 - Insertion of a wire (20 $\mu\text{m}$ diameter) into ocular surgery needle (50 $\mu\text{m}$ in diameter) .....	10
Figure 2.3 - Symmetrical location of strain gauge on a microgripper .....	12
Figure 2.4 - (a) Schematics of micro tri-axial force sensor chip. (b) Placement of Piezo-resistive strain gauge on the force sensor chip .....	13
Figure 2.5 – A fabricated PVDF sensor .....	14
Figure 2.6 – The schematic design of the two-axis PVDF force sensor .....	14
Figure 2.7 – The schematic design of a multi-axis capacitive microforce sensor .....	16
Figure 2.8 – Optical beam deflection for noncontact force sensing .....	17
Figure 2.9 - AFM for noncontact force sensing .....	17
Figure 2.10 – Properties of deformability of single wet fibres .....	18
Figure 2.11 – Typical stress-strain curve of an individual pulp fibre .....	19
Figure 2.12 - Different types of fibre bonds loading. (A) Shear mode. (B) Z-directional mode. (C) Torsional or tearing mode. (D) Peeling mode .....	20
Figure 2.13 - Schematic representation of the layer structure of a single wood fibre ....	22
Figure 2.14 - SEM micrograph showing fibril orientation of an individual wood pulp fibre .....	23
Figure 2.15 – Schematic illustration of transmission ellipsometry measurement .....	24
Figure 2.16 – Individual fibre flexibility measurement .....	26
Figure 2.17 - Process of manipulating and breaking an individual fibre-fibre bond .....	27
Figure 2.18 – Individual fibre-fibre bond strength measurement .....	27
Figure 2.19 - Handling of fibre-fibre bonds for nanotomography studies (a), Fibre specimen preparation for the diagonal compression test inside an SEM (b) .....	28
Figure 2.20 – Drop-on-fibre contact angle measurement .....	28
Figure 3.1 - Implementation of Microrobotic Platform A: 1, 2, and 3) XYZ-micromanipulators; 4) Rotary table; 5) XY-table; 6) Microforce sensor; 7) Microdispensor .....	33
Figure 3.2 – 3D model of Microrobotic Platform B .....	34
Figure 3.3 – Photograph of Microrobotic Platform B .....	35

Figure 3.4 - Conceptual design of the method for Z-directional strength measurement of IFFBs.....	37
Figure 3.5 - Schematic design of the force sensing module: 1) IFFB; 2) piezoelectric PVDF polymer film; 3) Connecting element; 4) Bond holder; 5) Mounting stage.....	38
Figure 3.6 - Implementation of the Sensor: 1) PVDF film; 2) Connecting element; 3) Bond holder; 4) Mounting stage.....	38
Figure 3.7 - A) Connecting element; B) Bond holder placed inside the Connecting element; C) Stack of Bond holders.....	39
Figure 3.8 - Implementation of the microrobotic platform. 1) and 2) XYZ-microgrippers, 3) L-shaped-micromanipulator, 4) L-shaped probe, 5) Rotary table, 6) Sensing module, 7) XY-table .....	39
Figure 3.9 – Reference microforce sensor .....	40
Figure 3.10 – Implementation of the calibration setup: 1) FT-S10000 sensor (reference sensor); 2) PVDF microforce sensing module; 3) SLC-1730 actuator; 4) PVDF film; 5) L-shaped connector.....	41
Figure 3.11 – Load application for calibration: a) zero load; b) full range load. ....	41
Figure 3.12 - Input signal sequence for PVDF microforce sensor calibration.....	42
Figure 3.13 – FT-S10000 sensor (reference force sensor) output vs actuator displacement.....	43
Figure 3.14 – PVDF microforce voltage output vs actuator displacement .....	43
Figure 3.15 – Linear calibration curve of the PVDF microforce sensor .....	44
Figure 3.16 – Positioning of the droplets on the plates (a) - Stack of bond holders (b) .	45
Figure 3.17 - IFFB manipulation near the bond holder (a) - IFFB mounting on the bond holder (b).....	46
Figure 3.18 - Mounted IFFB .....	47
Figure 3.19 - Z-directional force application to IFFB .....	47
Figure 3.20 - A representative Force-Time curve for the Z-Directional IFFB strength measurement.....	48
Figure 3.21 - Conceptual design of the method for microfibril angle measurement.....	49
Figure 3.22 – Motorized analyzer for transmission ellipsometry imaging .....	50
Figure 3.23 – Integration of the motorized analyser to Microrobotic Platform B .....	51
Figure 3.24 – Light source wavelength control – (a) Red light – (b) Green light – (c) blue light.....	51
Figure 4.1 - Effect of deformation rate on PVDF force sensor calibration curve .....	54

Figure 4.2 – Transmission ellipsometry images of a sample BSKP fibre .....	58
Figure 4.3 – Representation of the microfibril angle measurement .....	58
Figure 4.4 – Straightened fibre for microfibril angle measurement .....	59
Figure 4.5 – The reliable zones for microfibril angle measurement and comparison ....	60
Figure 4.6 – Average microfibril angle vs. strain in Zone A .....	61
Figure 4.7 – Average microfibril angle vs. strain in Zone B .....	61
Figure 4.8 – Average microfibril angle vs. strain in Zone C .....	62



## LIST OF TABLES

Table 2.1 – Morphological properties of fibres.....	18
Table 2.2 – Level of significance versus $df$ and $t$ .....	30
Table 4.1. Average velocity vs. actuation frequency.....	53
Table 4.2 - The calibration curves coefficients .....	54
Table 4.3 - Z-directional fibre-fibre bond strength of BSKP samples.....	56
Table 4.4 - Z-directional fibre-fibre bond strength of RBSKP samples .....	56
Table 4.5 – Summary of the measurements .....	57
Table 4.6 – Summary of the T-test analysis.....	57
Table 4.7 – Applied strain vs. micromanipulator movement.....	59
Table 4.8 – Average MFA value in the zones vs. strain .....	60

## LIST OF ABBREVIATIONS

2D	Two dimensional
3D	Three dimensional
AFM	Atomic Force Microscope
BSKP	Bleached Softwood Kraft Pulp
CCD	charge-coupled device camera
DOF	Degree of Freedom
FCT	Festo Configuration Tool
FLER	Fibre Load Elongation Recorder
FLER2	Second Generation of Fibre Load Elongation Recorder
FOV	Field of View
IFFB	Individual Fibre-Fibre Bond
LED	Light-Emitting Diode
MEMS	Micro-electro-mechanical systems
MEP	maximum extinction position
MFA	Microfibril Angle
NIR	Near infrared spectroscopy
PLA	Poly Lactic Acid
PVDF	Polyvinylidene Fluoride
RBSKP	Refined Bleached Softwood Kraft Pulp
SCU	Simple Control Unit
SEM	Scanning Electron Microscope
TUT	Tampere University of Technology
UV	Ultraviolet

## LIST OF SYMBOLS

$I$	Moment of inertia
$\varphi$	Microfibril Angle
$E$	Young's Modulus
$y$	Deflection
$F$	Force
$L$	Length
$S1$	First layer of the secondary wall of an individual wood fibre
$S2$	Second layer of the secondary wall of an individual wood fibre
$S3$	Third layer of the secondary wall of an individual wood fibre
$PA$	Angle (azimuth) between fibre axis and polarizer
$A$	Angle (azimuth) between polarizer and analyser
$I_0$	Intensity when the angle between polarizer and analyser is $0^\circ$
$I_{45}$	Intensity when the angle between polarizer and analyser is $45^\circ$
$I_{90}$	Intensity when the angle between polarizer and analyser is $90^\circ$
$I_{135}$	Intensity when the angle between polarizer and analyser is $135^\circ$
$\sin$	Sine function
$\cos$	Cosine function
$T_1$	Intermediate quantity in microfibril angle calculation
$T_2$	Intermediate quantity in microfibril angle calculation
$\arctan$	Inverse tangent function
$\arccos$	Inverse cosine function
$\Delta$	Phase retardation
$\lambda$	Wavelength

$N_a$	Size of sample A
$MX_a$	Mean of sample A
$SS_a$	Standard deviation of group A
$S^2$	Variance
$\sigma$	The standard deviation of the sampling distribution of sample-mean differences
$t$	Parameter t in T-test analysis
$df$	Mass of samples in T-test analysis
$P$	P value in T-test analysis
$X$	X axis
$Y$	Y axis
$Z$	Z axis
$FZ$	Z-directional force
$\Delta v$	Output voltage of the PVDF sensor
$P1$	The slope of the fitted line
$P2$	The offset of the fitted line
$\varepsilon$	Dielectric permittivity
$E_c$	Electric field
$d$	Piezoelectric coefficient
$T$	Applied stress
$S$	Strain
$s$	Elastic compliance
$\Delta l$	Length change
$l_0$	Initial length
$V_o$	Output voltage

$V_s$	Supply voltage
$C$	Capacitance
$DF$	Deformation rate

# 1. Introduction

Testing mechanical properties of micro and nanoscale materials has experienced a significant increase in importance with the development and industrialization of micro and nanodevices. This is evident in a recent survey, where as many as 600 papers published since 1920 were investigated [1]. According to the survey, more than 70% of the papers have been published in the last decade. Micro-testing is linked with robotics, since microscale materials can be grasped, handled, placed or tested by microrobots. Microrobotics, as a solution to testing and characterization of microscale objects, is a relatively new research field, dealing with movement, handling and manipulation of objects at microscale. Microrobotics is a technology discipline that refers to the design of systems capable of physically interacting in a controlled and prescribed manner within the microworld [2]. The capabilities of microrobotics - as a tool to interact with microscale objects- have been demonstrated in a quite wide range of applications during last two decades [3]. The use of micromanipulation in the industrial production and microassembly of complex miniature devices is an emerging area of application. In manufacturing, microassembly of miniaturized components has been performed using microrobotics [4] [5] [6]. Furthermore, precise micromanipulation and positioning of living cells have provided significant added value to the field of biomedical research. In medicine, active endoscopes [7] as tools in mini-invasive surgeries and smart pills [8] are other illustrations of microrobotic applications. In cell biology, microrobots are used to interact with living cells [9] [10] [11].

Paper is a network structure composed of various wood cells, mainly fibres, and fines. Fibres are cells having typical dimensions of 0.8 – 4.5 mm in length and 16 - 70  $\mu$  in diameter depending on their type [12]. Understanding the properties of papermaking fibres will contribute to the understanding of the paper properties as well. For instance, pulp and paper field researchers and engineers are using the microscale properties of paper in individual fibre and fibre bond level to develop numerical models on different scales from fibre bond to network level. The models can be used to derive directions for improving fibre and bond properties and for optimising the paper structure. Moreover, the mechanical properties and chemical composition of papermaking fibres are normally determined by bulk parameters. The average bulk parameters, however, do not provide a real possibility for predicting relevant fibre properties. Individual fibre level studies will improve the understanding of the influence of the paper chemical on the paper strength and can lead to more functional chemicals and also significant cost savings in product

development The interest in and the necessity of getting new information and data on papermaking fibres, fibre wall fine structures, and fibre-fibre bonds have increased during the recent years. In addition to the new measurement data, controlled mechanical treatment and chemical functionalization of individual paper fibres could lead to dramatic improvements in properties of fibre products. The aforementioned controlled functionalization, treatment and characterization of individual fibres can be studied only by developing new tools.

Micro and Nanosystems research group of Tampere University of Technology (TUT) has commenced utilization of microrobotics as a tool in mechanical microtesting and characterization of individual pulp and paper fibres in recent years. A microrobotic platform has been developed for individual fibre and bond level studies [13]. Several functionalities have been added to this platform during these years. The feasibility of performing multiple individual fibre and fibre bonds characterization experiments have been demonstrated such as individual fibre flexibility measurement [13], individual fibre-fibre bond making, manipulation, and breaking [14], individual fibre-fibre bond strength measurement [15] [16], wetting ability evaluation of individual fibres in terms of drop-on-fibre contact angle measurement [17]. This thesis work aims to add two functionalities to the microrobotic platform for experimental evaluation of Z-directional individual fibre-fibre bond strength and microfibril angle measurement.

### **1.1. Problem Statement**

Bond strength is the main mechanical property of individual fibre-fibre bonds (IFFB) attributed to contact area between fibres and adhesion capability of fibre surfaces [18]. In a paper network, fibre bonds transfer the load between fibres as interfibre joints and affect mechanical behavior of the entire network. To better understand the mechanical behavior of these network materials, individual fibre bonds should be characterized. Investigation of different loading modes of fibre bonds has been a substantial topic in pulp and paper area. Modes of loading a fibre bond are divided into four types: shear mode, z-directional or opening mode, torsional or tearing mode [19], and peeling mode [20]. It is desirable for papermaking companies and paper converting companies to obtain the Z-directional strength of pulp and paper both at the handsheet level and at the individual fibre bond level. To-date numerous efforts have been undertaken for experimental evaluation of bonds strength in different types of loading. Existing investigations and methods do not in general take the mode of loading into account [20]. Moreover, most of these methods are focused on the shear mode. Furthermore, the measurements generally show very high variability in most cases [21]. Due to increasing quality demands on paper and board products, it is important to consider not only the average value but also the distribution of bonding ability of different fibres [22] which requires a high throughput measurement method to fulfill the demand. Therefore, a reliable and high throughput method for the IFFB strength measurement in the Z-

directional mode of loading is required. This thesis work aims to address this need in research and industry by means of design and integration of a system for measuring Z-directional individual fibre-fibre bond strength to the current microrobotic platform.

Besides, paper scientists are interested in microfibril angle changes during and after application of the Z-directional force. In other words, there is interest in simultaneous measurement of microfibril angle and Z-direction bond strength in pulp and paper industries. To address this need, a microfibril angle measurement system is needed to be integrated to the microrobotic platform.

In summary, the chief objective of this thesis work is to integrate Z-directional individual fibre-fibre bond strength and microfibril angle measurement to the current TUT's microrobotic platform for characterization of fibrous materials which facilitates simultaneous measurement of individual fibre-fibre bond strength and microfibril angle.

## **1.2. Research Objectives and Expected Results**

According to the problem statement, the core objective of this thesis work is to develop methods -using microrobotics as a tool- for simultaneous measurement of Z-directional individual fibre-fibre bond strength and microfibril angle at the single fibre level. The core objectives of this thesis work can be summarized as follows:

1. A measurement method should be developed for Z-directional fibre-fibre bond strength measurement at the single fibre level, and the developed technology should be integrated to TUT's fibre characterization microrobotic platform.
2. A measurement method should be developed for automated microfibril angle measurement at the single fibre level, and the developed technology should be integrated to TUT's fibre characterization microrobotic platform.

Stemming from the exceptional scientific novelty, substantial improvements are expected in multiple areas, including the following:

- Z-directional fibre-fibre bond strength measurement will be facilitated at the single fibre level for the first time.
- Effect of certain modifications (e.g. adding paper chemicals or mechanical deformation of fibres) on Z-directional fibre-fibre bond strength of paper fibres can be investigated.
- Measurement of the microfibril angle can be performed while doing e.g. fibre manipulation or flexibility measurement.
- High throughput measurement of microfibril angle at the single fibre level will be facilitated.
- Simultaneous measurement of individual fibre-fibre bond strength and microfibril angle will be facilitated for the first time.



- Integration of the developed technologies to TUT's microrobotic platform will provide added value to the platform.

### **1.3. Research Method Explanation**

This thesis presents an experimental method for measuring the Z-directional individual fibre-fibre bond strength using microrobotics. In this work, a concept for measuring the Z-directional IFFB strength is presented. A bending Polyvinylidene fluoride (PVDF) force sensor as a sensing element is proposed for the measurement. Furthermore, the effect of deformation rate on the PVDF force sensor performance is studied. The PVDF force sensor is calibrated for different deformation rates. To demonstrate the functionality of the method, the effect of refining on the Z-directional strength of bleached softwood Kraft pulp fibre bonds is investigated.

Besides, microscopic transmission ellipsometry method is implemented on the microrobotic platform for microfibril angle measurement. This enables high throughput automatic microfibril angle measurements at the fibre level. The microrobotic platform is expected measuring Z-directional bond strength and microfibril angle separated and also synchronously.

### **1.4. Overview of the PowerBonds Project**

This thesis work is performed as a part of a PowerBonds (Enhancement of Fibre and Bond Strength Properties for Creating Added Value in Paper Products) project which is a WoodWisdom-Net project. It is accomplished in Micro and Nanosystems research group of the Department of Automation Science and Engineering at Tampere University of Technology. Understanding the importance of paper strength and taking steps towards reducing the grammage based on this understanding is the primary goal in this project. Tasks are defined and executed towards this goal on the dry and wet tensile strength of the printing and speciality papers and on the dry compressive strength of board which is relevant to packaging applications. Moreover, controlling the runnability in paper production is another goal of this project. In this project, microscopic characterization tools, novel experimental techniques working at a microscale, simulation tools and advanced pulp-processing technology are combined in order to understand the paper strength. The characterization tools are used to study the mechanical and morphological properties of papers at the single fibre level and handsheet level. The experimental tools, such as nano and micro-tomography, atomic force microscopy (AFM) and scanning electron microscopy (SEM), and micro- and nanorobotic technologies enable the characterization of mechanical and morphological properties of fibres and fibre bonds. In addition, improvement of the fibre strength and

bonding capability using novel mechanical and chemical fibre modifications is another core content of the project.

TUT's objective in this project is to develop novel systems and methods using microsystems technology for mechanical and morphological characterization of wet and dry individual fibres and fibre bonds to generate measurement data on wet and dry fibres and fibre bonds. This measurement data can be used to investigate the effects of fibre modifications. Moreover, the measurement data can be used to develop numerical models of paper on different scales from fibre bond to network level.

## 1.5 Collaboration

This thesis work has been a collaborative work by other researchers in the Micro- and Nanosystems Research Group of the Department of Automation Science and Engineering at Tampere University of Technology. The main contributions of the author have been as follows.

1. Conceptual design of the Z-directional IFFB strength measurement method.
2. Calibration of the PVDF microforce sensor for different deformation rates and analysis of the results.
3. Development of the Z-directional IFFB strength measurement method including fabrication of needed parts (except the PVDF film) and integration of the sensing element to the existed Microrobotic Platform A.
4. Performing the Z-directional IFFB strength measurements for unrefined and refined bleached softwood Kraft pulp (BSKP and RBSKP) fibres and analysis of the results.
5. Selection of the stepper motor and gears for microfibril angle measurement.
6. Finalization of the mechanical design of the Microrobotic Platform B.
7. Design, fabrication, and integration of the stepper motor connector to the Microrobotic Platform B.
8. Performing microfibril angle measurement for free BSKP fibres.
9. Performing microfibril angle measurement for a stretched BSKP fibre to analyse the effect of strain on MFA and analysis of the results.

## 1.6. Thesis Outline

The rest of the thesis is organized as follows:

**Chapter 2** includes the theoretical background and framework. This chapter is divided to several subsections to cover all required background in the following sections. A general overview of microrobotic manipulation systems is described. Piezoelectric effect as the working principle of used Microactuators and the PVDF

microforce sensor is described. Microforce sensing methods are explained briefly in the second section of Chapter 2 of the thesis. Paper fibre properties are described in the next section. The focus is on Z-directional strength and microfibril angle. Hence, different experimental evaluation methods of Z-directional strength and microfibril angle are described and pros and cons of each are explained. The theory of the implemented microfibril angle measurement method is described in this section. Existing functionalities of TUT's microrobotic platform are also explained in this chapter. T-test analysis is also briefly described in this chapter.

Research materials and methods including Z-directional bond strength measurement design and implementation, effect of deformation rate on PVDF film microforce sensor response, and microfibril angle measurement design and implementation are explained in **Chapter 3**.

Results of the executed experiments and analysis of the results are presented in **Chapter 4**.

**Chapter 5** includes the conclusion and future works.

## 2. Theoretical Background and Framework

This chapter includes the theoretical background and framework of this thesis. A general description of the microrobotic manipulation systems is presented in Section 2.1. Piezoelectric effect as the working principle of used Microactuators and the PVDF microforce sensor is described in Section 2.2. Experimental microforce sensing methods and pros and cons of each method are explained in Section 2.3. As the application domain of this thesis work is pulp and paper fibre characterization, paper fibre properties are described briefly in Section 2.4. Different loading modes of individual fibre bonds are presented and Z-directional fibre-fibre bond strength is described in more details. The measurement techniques of bond strength are described in Subsection 2.4.1. Microfibril angle definition and measurement techniques are explained in Subsection 2.4.2. Existing capabilities of TUT's microrobotic platform for fibre characterization studies are explained in Section 2.5. Finally, T-test analysis is briefly explained in Section 2.6 as it is used in the interpretation of the results of the Z-directional measurements.

### 2.1. Microrobotic Manipulation Systems

Microrobotics is a relatively new field of robotics with two decades of history, dealing with miniature robots enabling movement, handling and manipulation of components at microscale. Microrobotics is a key enabling technology in assembly, integration, quality control, testing and characterization of micromaterials, devices, and systems. As microscale materials cannot be manually grasped, handled, placed or tested in high throughput, characterization and testing of microscale materials is linked with microrobotics. The basic idea of Microrobotic manipulation systems, as a solution to testing and characterization of microscale objects, is to adapt the manipulator for micro meter scale material handling effectively as industrial manipulator robots in macro scale material handling. However, due to the very special physical environment at microscale, the two-decade progress in microrobotics has mostly been on solving the physics induced problems such as:

1. The uncertain dominant surface forces due to van der Waals, electrostatic, capillary and other adhesion forces that often bring handling difficulties and

failures, such as objects sticking to the handling tool, failed picking-and-placing, excessive adhesion between object and substrate, etc.

2. The complexity and variety in shapes and material properties of natural objects, such as living cells and natural fibres, bring challenges to perception and handling.

Significant progress has been made on this front in recent years. The progress in microrobotics enables a wide range of applications from the biomedical applications to material testing and microassembly of miniaturized products. Microrobotics can be applied in this wide range of applications for the general purpose of analysis of micro-nano objects, assembly of micro-nano systems, and handling, modification, and connection of micro-nanostructures. [23]

### 2.1.1. Components of Microrobotic Manipulation Systems

Microrobotic manipulation systems involve handling of parts that have dimensions in microscale. Microrobotic manipulation systems are composed of the components that can functionally accomplish or support the accomplishment of one or all of the following tasks:

- Grasping of a target microscale object.
- Manipulation and placement of microscale objects.
- Recognition of the part and object before, during and after operations such as micro-testing, assembly, and micromanipulation.
- Planning and control of the actuators and grippers to perform the tasks.
- Sensing elements to probe the properties of the micro objects.

The main purpose of the state-of-the-work research in microrobotics has dealt with addressing the automation of these activities [4]. Based on the aforementioned tasks, the main components of a microrobotic manipulation system can be categorized functionally into four main areas:

1. **Micromanipulator as the positioning device:** this component of micromanipulation systems focuses on the ability to actually perform the micromanipulation task using stages, microactuators, and other positioners.
2. **Vision system:** This fundamental component of micromanipulation systems deals with visually sensing the positions of the target parts, end-effectors, associated pins, obstacles, etc. Vision system includes some kinds of microscopies as “eyes” of the system like optical microscope, SEM, etc.
3. **End-effector:** This component provides the interface between a micromanipulator and microscale objects. End-effectors include grippers,

cantilevers, tweezers, and injecting capillaries. This component acts as “fingers” of the micromanipulations system.

4. **Sensing element:** This component includes different types of sensors (force, displacement, tactile, strain, etc.) to measure the state of manipulations and/or to probe the properties of the objects. [23]

### 2.1.2. Applications of Microrobotic Manipulation Systems

Progress in various key technologies such as vision systems, actuation, measurement, system design and fabrication, calibration and control, communication, and human-machine interface enables the utilization of microrobotic manipulation systems in different application cases [23]. The application areas vary from industrial micro mechatronics to biomedical applications such as cell engineering.

In response to the market demand, greater miniaturization and the integration of complex features are needed in many industrial components. There are many applications in the fields of optics, mechanics and electronics. In micro-optics, a major example is the construction of optical guides or switches for telecommunication applications. One other application is in the relative positioning and attachment of a lens to the tip of an optical fibre (generally of diameter 125 to 250  $\mu\text{m}$ ). In micro-mechanics, implantable miniature valves are developed. Mechanisms such as the micro-gears, micro-motors, micro-dosing systems or micro-bearings are micro-manipulated (Fig. 2.1). Microelectronics is also a rich source of industrial applications of micromanipulation. Applications include microassembly of microelectronic components on a circuit board or miniature electron guns. With the available technology, using micromanipulation systems in assembly of all these products guarantee the level of accuracy and required consistency of quality; however, the cost of manipulation operations becomes very high. [3]

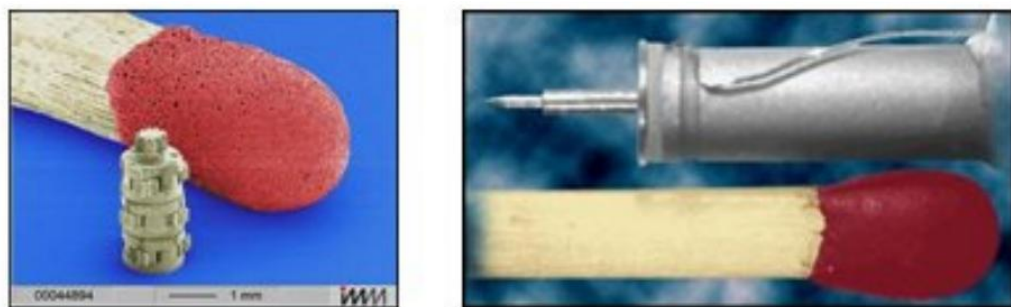


Figure 2.1 - Examples of micro-mechanisms: micro-gear (left); micro-motor (right)  
[3]

Micromanipulation systems are expected to lead the progress of novel technologies especially in the medical field such as drug delivery systems and micro-nano surgery

inside the human body [24]. In medicine, many relevant tasks are performed manually. For instance, the insertion of a wire into the barrel of an ocular surgery needle is currently performed manually (Fig. 2.2). The diameter of wire is 20  $\mu\text{m}$  which must first be dipped in glue before being inserted into the hole. The feasibility of performing this task with microrobotics in fully-automated mode has been demonstrated.

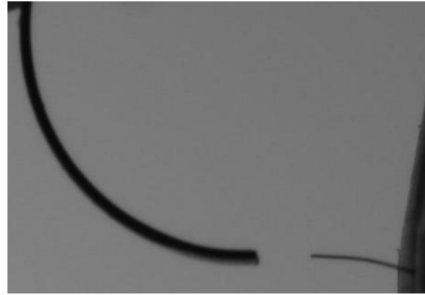


Figure 2.2 - Insertion of a wire (20  $\mu\text{m}$  diameter) into ocular surgery needle (50  $\mu\text{m}$  in diameter) [3]

Another application domain for micromanipulation systems is living cell studies. The target in this field is to understand the cell function using engineering. This academic field also aims to reconstruct the cell function and functional control of tissue [23]. The exploration of the living world on the smallest scales involves the development of observation methods, characterization, processing or manipulation of organisms (humans and animals) on very small scales. Given the characteristic dimensions of live cells (from one micron to a few hundred microns), the fields of micromanipulation and cellular biology are intrinsically linked.

Microrobotic manipulations systems facilitate characterization of materials at microscale which is an emerging application field. In general, material characterization includes testing materials to extract morphological and mechanical properties. The mechanical testing at microscale is classified to static and dynamic tests. Tension, compression, bending, torsion, and nanoindentation tests are examples of static tests. Dynamic tests include fatigue and resonant tests. The state-of-the-work micromanipulation systems facilitate multiple material characterization applications such as micro-testing of micro-electro-mechanical systems (MEMS). [1]

## 2.2. Piezoelectric Effect

Piezoelectricity is the electric charge that accumulates in certain solid materials e.g. crystals in response to applied mechanical stress. The direct piezoelectric effect comes as a result of the displacement of positive and negative charges within a crystal lattice following the application of mechanical stress. In other words, when mechanical stress is applied to the piezoelectric material, it generates charge. Direct piezoelectric effect is utilized in piezoelectric sensor applications. Similarly, there is an inverse

piezoelectric effect where a deformation occurs in the piezoelectric material as the result of electric field application. Inverse piezoelectric effect is used in piezoelectric actuator applications. Thus, piezoelectric materials display electromechanical coupling. [3]

In the case of direct piezo electric effect, the expression for electric displacement as a function of applied mechanical stress can be written as follows.

$$D = d \cdot T \quad (2.1)$$

Where  $D$  is the electric displacement,  $d$  is the piezoelectric coefficient and  $T$  is the applied stress. The piezoelectric material would be in electric field, and the total expression for electric displacement is as follows.

$$D = d \cdot T + \varepsilon \cdot E_c \quad (2.2)$$

Where  $\varepsilon$  is the dielectric permittivity and  $E_c$  is the electric field.

In the case of inverse piezo electric effect, the expression for strain ( $S$ ) as a function of applied electric field is as follows.

$$S = d \cdot E_c \quad (2.3)$$

The piezoelectric material would be under other mechanical deformations. Thus, the total expression for strain is as follows.

$$S = d \cdot E_c + s \cdot T \quad (2.4)$$

Where  $s$  is the elastic compliance. To wrap up,  $S$  and  $T$  can be written in matrix form as follows.

$$\begin{bmatrix} S \\ D \end{bmatrix} = \begin{bmatrix} s & d \\ d & \varepsilon \end{bmatrix} \cdot \begin{bmatrix} T \\ E_c \end{bmatrix} \quad (2.5)$$

### 2.3. Microforce Sensing

Force sensors are devices for measuring interaction forces. In most of the cases, the sensing element of force sensors deforms when external forces are applied. The deformation can be detected by measuring the change in certain properties of the sensing element such as resistance in strain gauges or capacitance in capacitive sensors. The relationship between the output signal resulted from the deformation and a known force is established by means of calibration process. In microforce sensors, the magnitude of forces may range from 1  $\mu\text{N}$  to several  $\text{mN}$  [25]. Indeed, precise microfabrication techniques have been applied to fabricate such sensitive and stable sensing elements. To-date, strain gauge, piezoelectric, capacitive, and optical sensors are



the most typical microforce sensors which are briefly introduced in the following sections. Strain gauges, piezoelectric force sensors, and capacitive force sensors are types of contact force sensors which measure the force through contact with the micromanipulator. In contrast, optical sensor is used in noncontact force measurement. Each of the four types of force sensing techniques has its advantages and disadvantages. Certain techniques are more suitable for a particular application than others.

### 2.3.1. Strain Gauge

When force is applied to a strain gauge, it deforms and the deformation changes its resistance. The change in resistance is remained until its original shape is restored. An electrical circuit such as Wheatstone bridge is commonly used to measure the resistance change. The resolution of strain gauges is a function of the amplifier noise level and the bridge configuration of the sensor. The typical resolution of a conventional strain gauge is above 1 mN. However, force sensor consisting of strain gauges is designed with much lower resolution of 0.5 nN [26] for the force control in micromanipulation. Strain gauges are usually made of a metal foil or of a semiconductor material. Semiconductor strain gauges are more sensitive than metal types.

Strain gauge is often integrated to the micromanipulator in microrobotic applications. However, it is often challenging to place the strain gauge in its optimal position due to the size of micromanipulator. A symmetrical method is developed to place strain gauges on a microgripper structure [27]. In this case, two pairs of strain gauges are mounted on the microgripper, so that one strain gauge of the pair measures compression while the other one measures tension. Better thermal compensation is the result of the symmetrical configuration. The schematic mounting of the strain gauges in the microgripper structure is shown in Fig. 2.3.

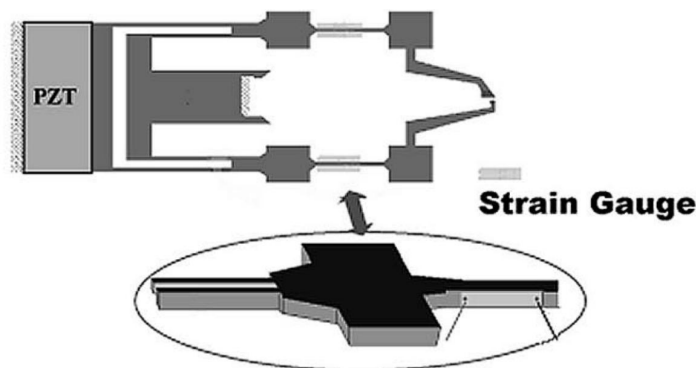


Figure 2.3 - Symmetrical location of strain gauge on a microgripper [27]

Multi-axis sensing can be achieved with a proper microsensor design. As an illustration, a microforce sensor is designed and fabricated which enables real-time tri-axial force measurement [28]. The schematic design of the force sensor chip is

illustrated in Fig. 2.4. Four cantilevers are used for center mass suspension. Each cantilever has two piezo-resistive strain gauges.

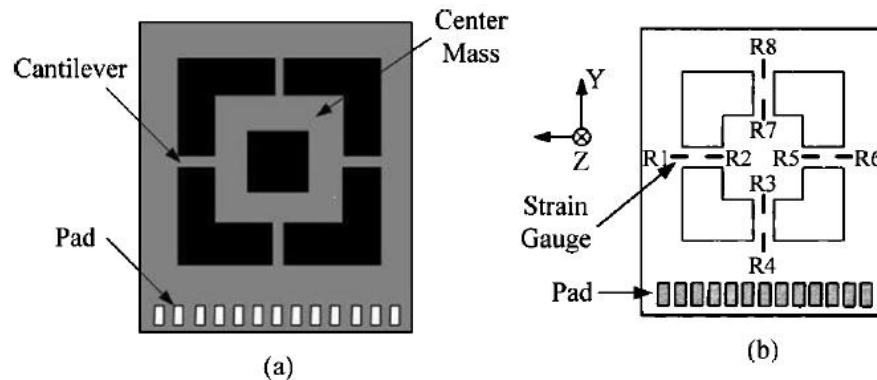


Figure 2.4 - (a) Schematics of micro tri-axial force sensor chip. (b) Placement of Piezo-resistive strain gauge on the force sensor chip [28]

The main drawback of using strain gauges in microrobotic applications is the required large deformations for the measurement. In fact, these large deformations cause geometric changes into the force measuring path and also affect the frequency response of the measuring system. These issues introduce measurement errors such as nonlinearity and hysteresis.

### 2.3.2. Piezoelectric Force Sensor

According to piezoelectric effect, when force is applied to a piezoelectric force sensor a voltage is generated. The stiffness of piezoelectric materials is quite high which is comparable to steel stiffness. This results in much smaller deformation of the sensing element in comparison with a strain gauge. Hence, the geometry change is highly reduced during the measurement compared to a strain gauge. This enables force measurement in many applications where a rigid sensing device is needed such as mechanical force measurement of a living cell. The high rigidity of piezoelectric force sensors also provides an inherently high natural frequency and short rise time. The measurement of extremely fast events is doable with piezoelectric force sensors due to their high natural frequency and short rise time. [25]

The polyvinylidene fluoride (PVDF) film is the most widely used piezoelectric force sensor. PVDF is applicable in a wide range of frequencies. High mechanical strength and high sensitivity are the other upsides of PVDF. PVDF microforce sensors have been used in a wide range of applications. A PVDF force sensor is designed and fabricated which can be integrated into a tweezers-type microgripper [29]. The fabricated PVDF force sensor is schematically illustrated in Fig. 2.5. A 28- $\mu\text{m}$  thick PVDF film is sandwiched between two parylene layers. The PVDF film is coated with 6  $\mu\text{m}$  parylene layer for thermal insulation, enhancement of the mechanical stiffness and isolation of

the nickel electrode from the environment. The nickel electrodes provide electrical output to an amplifier. This PVDF sensor enables the microgripper to sense gripping forces with magnitudes under  $100\ \mu\text{N}$ .

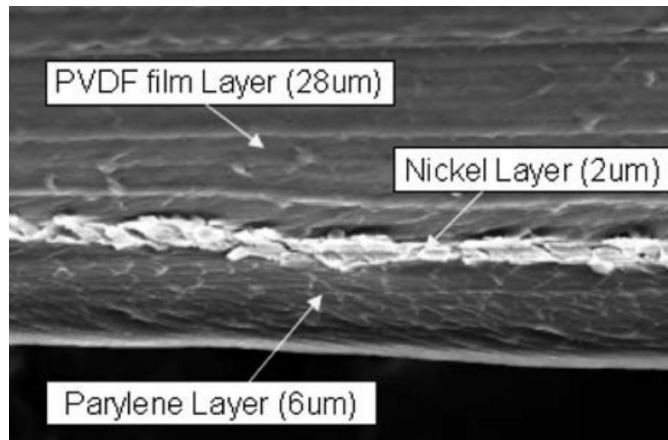


Figure 2.5 – A fabricated PVDF sensor [29]

A PVDF sensor can be used in microrobotic applications either directly installed on the grasping surface of a gripper [29] or integrated into a probe tip to detect the contact force exerted at the tip. For instance, a microinjection pipette is bonded on the tip of a PVDF force sensor to characterize the mechanical properties of the membrane of zebrafish eggs [30]. A two-axis PVDF force sensor with submicron resolution is designed to provide decoupled microforce measurement in X and Y directions [31]. The schematic design of the two-axis PVDF force sensor is shown in Fig. 2.6.

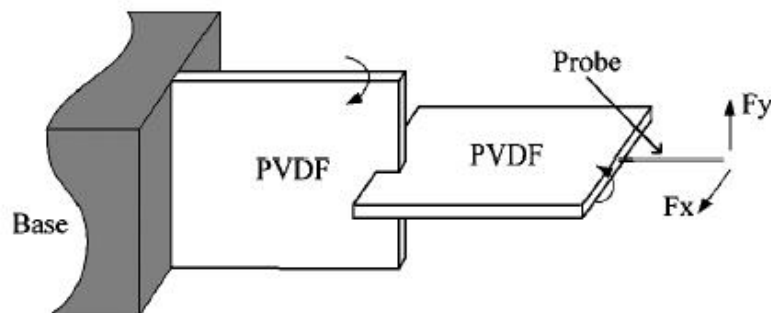


Figure 2.6 – The schematic design of the two-axis PVDF force sensor [31]

The drawback of the piezoelectric sensors is that the electrical signal generated by the piezo element falls rapidly after the application of the force. Due to this characteristic, piezoelectric sensors are not suitable for detecting static force [32]. Strain gauges and capacitive force sensors are applicable for static force measurement.

### 2.3.3. Capacitive Force Sensor

When force is applied to a capacitive force sensor, the capacitance between two metal plates is changed. The change in capacitance is either by change in the distance between the plates or the effective surface area of the capacitor. Since the capacitance between two parallel plates is a function of the plate area, the distance between the plates, and the permittivity of the dielectric medium, the change in the mentioned parameters result in change in capacitance. Capacitive force sensors are more stable and sensitive in comparison with strain gauges and piezoelectric force sensors. Moreover, the capacitive force sensors exhibit no hysteresis [33].

In a differential capacitive microforce measurement, two capacitors with a shared moving membrane and two fixed membranes are arranged in a parallel circuit structure. The voltage difference due to changes in two capacitors is measured. This is the basic idea of comb structured capacitive microforce sensors in which many (more than two) capacitors are connected in parallel and the voltage difference due to changes in all capacitors is measured. Improved linearity and sensitivity can be achieved Using comb structure capacitive microforce sensors of capacitive microforce sensors. The basic equation of differential capacitive microforce sensors is as follows.

$$V_o = V_s \cdot \frac{C_1 - C_2}{C_1 + C_2} \quad (2.6)$$

Where  $V_o$  is the output voltage,  $V_s$  is the supply voltage, and  $C_1$  and  $C_2$  are capacitances.

Capacitive force sensors have been widely used for biological materials characterization through force measurement. A microforce sensor capable of sensing forces in two axes is used to study the mechanical properties of mouse zona pellucida during fertilization [34]. The design of the sensor is shown in Fig. 2.7. The body of the sensor consists of a fixed outer frame and a movable inner structure. The outer and inner parts are connected with four springs. A probe is attached to the inner frame. When a force is applied to the sensor probe, the probe moves the inner structure which leads to change in the size of the gap between each pair of comb capacitors. The change in the size of the gap results in change in the total capacitance. The applied force can be calculated based on the change in capacitance. The capacitors are configured such that forces in the x and y directions can be determined. As shown in Fig. 2.7, comb drives 1, 3, 4, and 6 are for resolving forces in the x direction, while comb drives 2 and 5 are for the y direction.

In many micromanipulators, the manipulator is too small so that force sensor cannot be integrated into the manipulator. For these cases, noncontact sensing is needed. Optical sensors as effective sensors for noncontact force measurement are used in these cases.

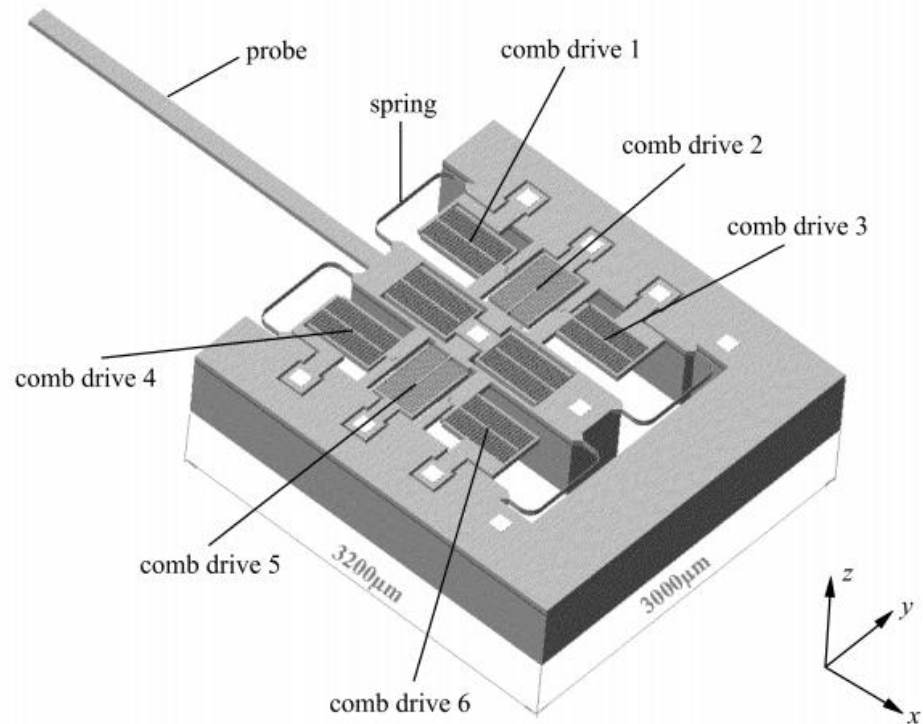


Figure 2.7 – The schematic design of a multi-axis capacitive microforce sensor [34]

#### 2.3.4. Optical Force Sensor

Optical beam deflection is utilized for microforce sensing in optical force sensors. The main advantage of optical force sensors is that they can be used in a noncontact mode. Resolution down to nanonewtons is achievable with this method. One application of this technique is the atomic force microscope (AFM) [25]. The idea of noncontact mode sensing technique based on optical beam deflection is shown in Fig. 2.8.

An AFM mainly consists of a manipulator integrated with nanoscale force sensing to characterize features on surfaces from the micrometer scale to the nanometer scale. AFM can also be used as a nanomanipulator for manipulation of nanoparticles [35]. The noncontact sensing technique using an AFM is illustrated in Fig. 2.9. During the scanning of the AFM tip over a sample, interatomic forces occur between the tip and the sample. This small force causes deflection of the cantilever, and is measured by a laser diode and a photodiode. Light from a laser diode is focused on the tip of a cantilever and deflected onto a quad photodiode. As the AFM scans a surface, the cantilever bends and twists due to applied forces to the AFM tip. The laser beam on the quad photodiode will move accordingly. The four voltage outputs from the photodiode are used to measure changes in the deflection of the beam [36].

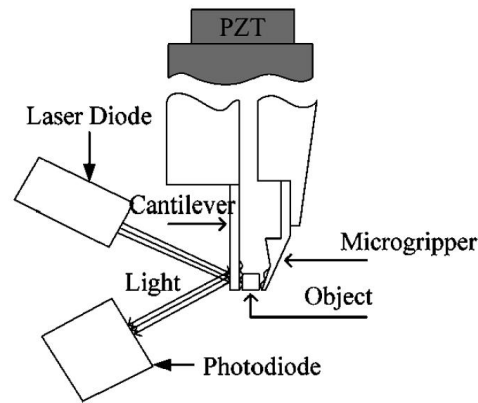


Figure 2.8 – Optical beam deflection for noncontact force sensing [25]

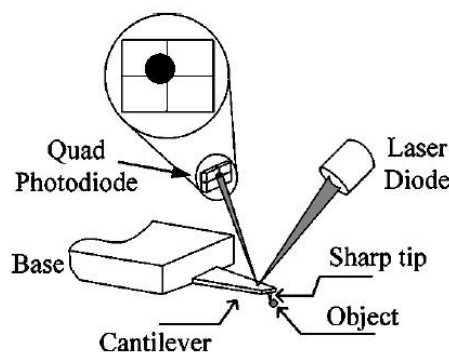


Figure 2.9 - AFM for noncontact force sensing [35]

The first disadvantage of using a cantilever type measurement is the range limitation. The photodiode can only detect deflection within a small range. Moreover, lack of accuracy in certain applications is another drawback of using AFM.

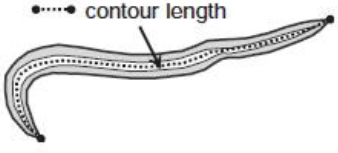
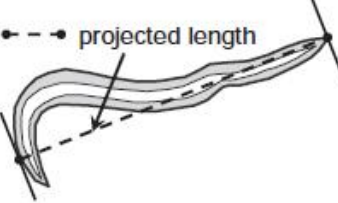

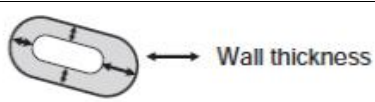
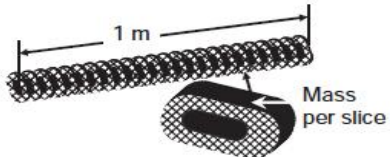
## 2.4. Paper Fibre Properties

As stated earlier, this thesis aims to develop methods for experimental evaluation of Z-directional fibre-fibre bonds strength and microfibril angle. Z-directional fibre-fibre bonds strength is a mechanical property in bond level, and microfibril angle is a morphological property which highly affects the mechanical properties of individual fibres. These features are explained in this section.

Paper is a network structure composed of various wood cells, mainly fibres, and fines. Fibres are cells having typical dimensions of 0.8 – 4.5 mm in length and 16 - 70  $\mu\text{m}$  in diameter depending on their type [12]. Understanding the properties of papermaking fibres will contribute to the understanding of the paper properties as well. Accordingly, pulp and paper related industries and research groups are interested in characterization of the individual fibres and fibre-fibre bonds. The characteristics of fibres are generally divided into two groups of morphological and mechanical properties. Morphological properties of fibres include fibre length, fibre width, fibre

curl, thickness of cell wall, coarseness, shape of fibre. These features are shown in Table. 2.1. [37]

Table 2.1 – Morphological properties of fibres [37]

Fibre property	Average of	Explanation
Contour length	Length of straightened fibre	
Projected length	Length of curled fibre	
Width	Dimension of cross section	
Curl	Extent of curling of fibre	$CU/\% = \left( \frac{\text{contour length}}{\text{projected length}} - 1 \right) \cdot 100$
Wall Thickness	Thickness of fibre wall	
Coarseness	Mass per unit length	

The prevailing mechanical features of fibres in wet state are collapsibility, flexibility, and conformability. Needed compression force to collapse the fibre laterally is an index of collapsibility. Flexibility of a fibre is the inverse of its bending stiffness. A bending force is applied to a single fibre while two ends of fibre are clamped, and the deflection of the fibre is measured. These features are illustrated schematically in Fig. 2.10. [37]

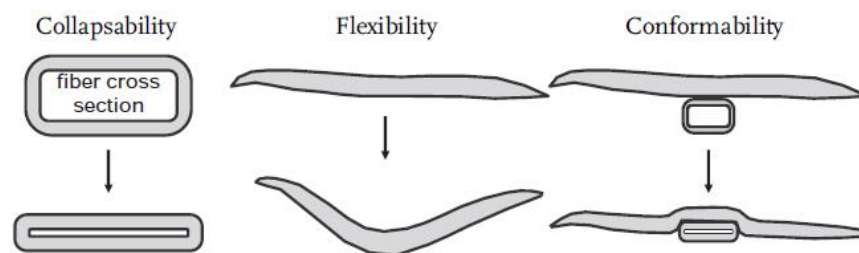


Figure 2.10 – Properties of deformability of single wet fibres [37]

Furthermore, the deformability of fibres in dry conditions is a matter of interest. In the context of deformability, highly informative data may be acquired from the stress-strain characteristics. The most commonly applied type of deformation is elongation which provides the informative data such as modulus of elongation, breaking load, and stretch at break. The stress-strain curve of an individual fibre is presented in Fig. 2.11. [37]

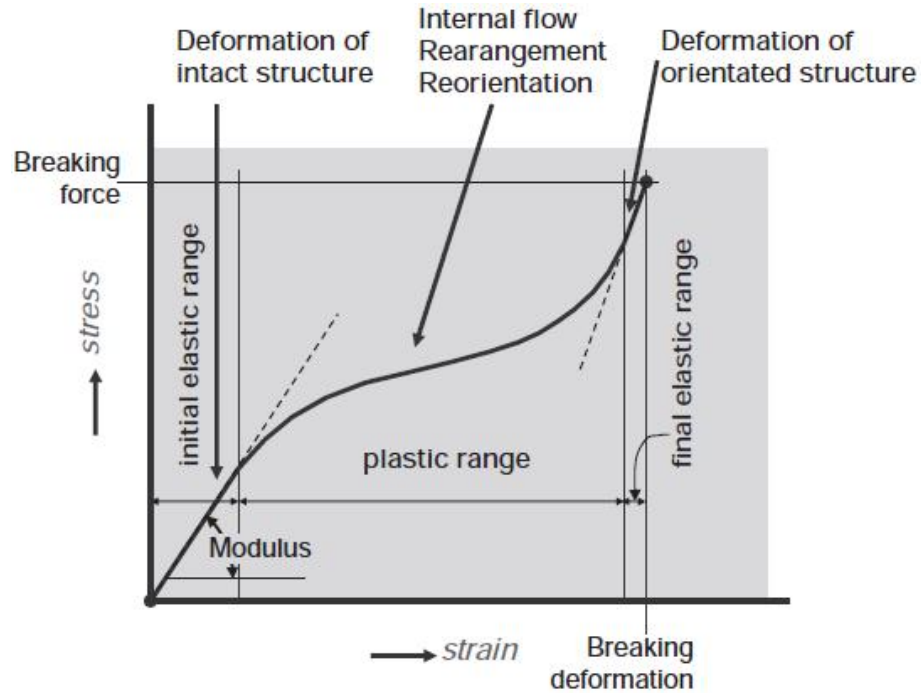


Figure 2.11 – Typical stress-strain curve of an individual pulp fibre [37]

#### 2.4.1. Z-Directional Individual Fibre-Fibre Bond Strength

Individual fibres and fibre bonds are construction units of paper/board sheets. Mechanical properties of paper/board are heavily influenced by mechanical properties of individual fibre-fibre bonds (IFFB). Bond strength is the main mechanical property of IFFBs attributed to contact area between fibres and adhesion capability of fibre surfaces [18]. In a paper network, fibre bonds transfer the load between fibres as interfibre joints and affect mechanical behavior of the entire network. Although paper is already known for almost 4000 years, the process of bonding two fibres together is still an open discussion. During the fabrication cycle of paper, single pulp fibres approach each other and form bonds during the drying process. The mechanism of forming bonds between two single fibres is up to now a speculative issue [38]. There are several mechanisms suggested that play a significant role in forming fibre-fibre bonds that lead to fibre network. Mechanical interlocking, hydrogen bonds, electrostatic interactions, interdiffusion, and induced dipoles are the five mechanisms proposed in literature for



forming fibre-fibre bonds [38]. To better understand the mechanical behavior of these network materials, individual fibre bonds should be characterized.

Due to different responses of paper to different applied forces, there is no unique measure or definition of paper strength [39]. Therefore, investigation of different loading modes of fibre bonds has been a substantial topic in pulp and paper area. Modes of loading a fibre bond are divided into four types: shear mode, z-directional or opening mode, torsional or tearing mode [19], and peeling mode [20]. Aforementioned types of fibre bonds loading are shown in Fig. 2.12.

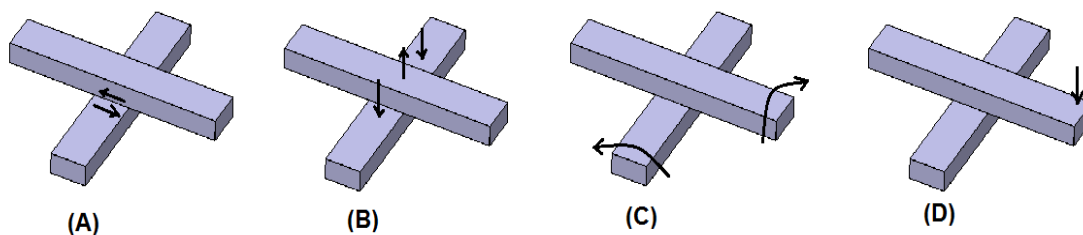


Figure 2.12 - Different types of fibre bonds loading. (A) Shear mode. (B) Z-directional mode. (C) Torsional or tearing mode. (D) Peeling mode. [40]

It would be desirable for papermaking companies and paper converting companies to obtain the Z-directional strength of pulp and paper both at the handsheet level and at the individual fibre bond level [41]. The Z-directional properties affect compressive properties which highly influence the performance of structural paperboard products [42]. In a paper mill, highly viscous materials are applied to the paper in sizing presses and coaters in printing and coating operations. In case when the Z-directional bonding strength of a paper sheet is low, the sheet can be pulled apart in the Z-direction during applying and drying these materials which causes build-up on the applicators and dryers. However, if the value of the Z-directional strength is too high, certain properties such as opacity, folding stiffness and tear strength will be reduced [41].

In pulp and paper research, one approach is to understand the paper and board behaviour using numerical modelling. To improve the prediction capability of these models, statistical data on various properties, such as the Z-directional strength of IFFBs are needed. Thus, there is a large interest in pulp and paper specialists to be able to obtain the Z-directional strength of fibre bonds.

Multiple methods for the experimental investigation of the IFFB strength have been proposed both at the handsheet level and at the individual fibre bond level until today. Three different methods at the handsheet level including the z-directional tensile test, the delamination test [41], and the Scott bond test [43] have been used to measure the internal bond strength of papers; however, a comparison of these methods does not show high correlation between the results [41]. There are several drawbacks in handsheet level methods. First, the results include the fibre-fibre bonding energy together with other energies. Moreover, these methods provide only inaccurate estimates

on the average values of bond strength. Different modes of loading are coupled in these measurements. Considering these issues in handsheet level measurements, methods are needed to measure the bond strength at a fibre level.

Methods which are proposed to measure the IFFB strength at a fibre level are briefly described as follows. Fischer et al presented a test setup for direct mechanical testing of fibre bonds [19]. Using their method, both shear and tearing modes of strength of fibre bonds can be measured. Button evaluated the strength of cellophane fibre bonds using an Instron testing machine and fibre load elongation recorder (FLER) [44]. Stratton and Colson measured the bond breaking load and the bonded area of several types of fibre bonds using FLER2 (second generation of FLER) and Page's polarized light scattering technique [45]. Schmied et al used conventional atomic force microscopy (AFM) technique to measure fibre bonding force in peeling mode [38]. The behavior prior to the failure is analyzed and correlated to the true bonded area. Saketi and Kallio have applied microrobotics for IFFB strength measurement [16]. Both ends of one fibre are fixed by micro grippers while one end of the other fibre is pulled by a load cell. A method for fabricating and testing of fibre bonds in shearing mode and also a peeling mode of loading is proposed by Magnusson et al in [20]. The method was applied to investigate the strength of Kraft pulp fibre bonds with different geometries. There are some disadvantages in the fibre level methods. These methods are generally slow and laborious. Furthermore, the measurements generally show very high variability in most cases. Most of these methods are focused on the shear mode. There is not any proposed method to measure Z-directional fibre-fibre bond strength at a fibre level.

#### 2.4.2. Microfibril Angle

Pulp fibres are made of one primary wall enveloped in lignin to form the middle lamella and three secondary walls, S1, S2, and S3 layers. All the three secondary walls are concentric and composed of cellulosic microfibrils embedded in an amorphous matrix of hemicelluloses and lignin. The most important wall is the middle layer S2, since it contains 80–95% of the fibre material, so that a wood pulp fibre can be approximately described by the S2 layer. The crystalline microfibrils of the S2 layer trace a steep spiral around the fibre axis, and the microfibrils of the front and back walls of the S2 layer are crossed. The angle between the fibrillar direction and the fibre axis is termed the microfibril angle of the fibre ( $\phi$  in Fig. 2.13). The layer structure of a single wood fibre is shown in Fig 2.13. [46]

The microfibril angle (MFA) is an ultra-structural parameter to characterise wood cell walls. It affects especially the axial strength properties of a fibre. Axial strength is increased but elongation decreased with decreasing angle. The elastic modulus and the shrinkage of the fibre are also affected by the microfibril angle. It also affects the transverse properties of fibres, including the swelling behaviour. The final fibre wall

structure depends also on stock preparation processes such as refining, and formation of the fibre network. [47]

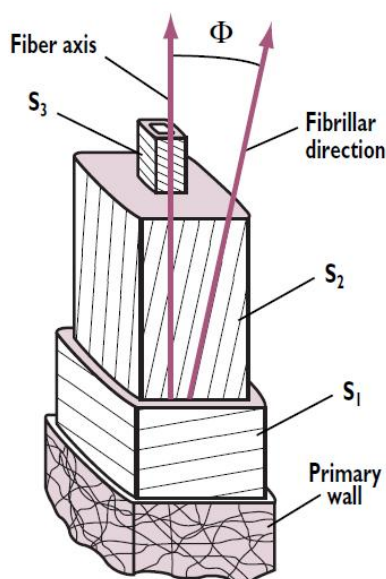


Figure 2.13 - Schematic representation of the layer structure of a single wood fibre [46]

Several methods have been developed and applied to determine microfibril angle (MFA). These methods can be categorized into two types. The first category of these methods includes those which are microscopy-based and use individual fibres to measure MFA. In contrast, bulk wood samples are used to measure MFA in the second category. X-Ray diffraction and near infrared (NIR) spectroscopy are the most referred techniques in this category.

Polarized light is used in multiple methods of microscopy-based techniques. Due to the fact that cellulose is partially crystalline, individual fibres show birefringence property when viewed between two crossed polarising filters. An individual fibre is rotated relative to the fibre axis until the bright cell wall becomes dark which is called maximum extinction position (MEP). Average MFA is the difference between the fibre axis and the MEP. The main difficulty with this technique is that an individual fibre has two walls which make it complicated to describe the state of the emerging light. Several methods are proposed to solve this issue. Preston [48] cut the tracheid longitudinally to leave only one wall. Page [49] overcame the same problem by filling the cell lumen with mercury and viewing reflected light using epi-illumination. Donaldson [50] used the holes formed by bordered pit apertures, where the pit membrane has been removed by maceration, to view the single cell wall on the opposite side of the cell. Verbelen & Stickens [51] used confocal bifluorescence microscopy which does not need single-wall cells. Batchelor et al. [52] proposed a method using polarization of reflected light to determine MFA. Ye & Sundström [46] applied spectroscopic imaging ellipsometry to determine MFA and fibre wall thickness. This technique does not require single cell

walls and does not need sample pre-treatment. In addition, this method is simple, fast, and convenient for automated measurement.

Several microscopy-based techniques are proposed which directly or indirectly visualise the orientation of the microfibrils such as scanning electron microscopy (SEM) [53], fluorescence microscopy [54], micro-Raman spectroscopy [55], confocal microscopy [56], and transmission electron microscopy (TEM) [57] [58]. An SEM micrograph which shows the microfibril orientation of an individual wood pulp fibre is presented in Fig. 2.14.

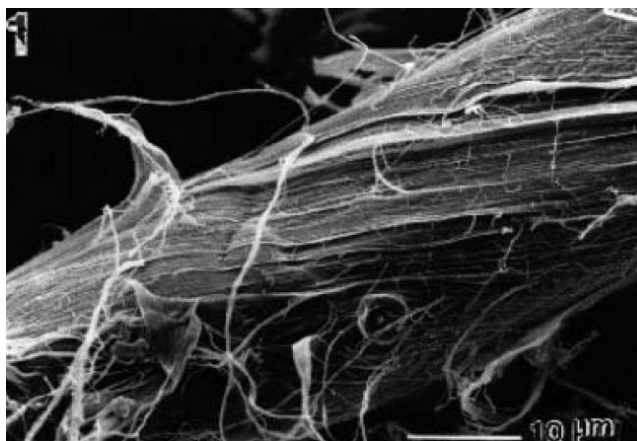


Figure 2.14 - SEM micrograph showing fibril orientation of an individual wood pulp fibre [59]

The most widely used method for MFA measurement is currently X-Ray diffraction. Average MFA in bulk wood can be obtained with multiple X-Ray Diffraction methods. Utilizing diffraction from 002 planes has been used [60] in which average MFA can be indirectly obtained. Furthermore, direct X-Ray scattering technique has been applied using diffraction from 040 planes for measuring MFA [61].

Near infrared (NIR) spectroscopy is used to predict MFA from bulk wood surfaces scanning on the radial longitudinal face of increment cores [62].

Polarized light microscopy has been widely applied in measuring the MFA. As described earlier, most of the methods require some kind of laborious sample pre-treatment. However, a method requiring no preparation steps or special sections has been reported as well [46]. This method is called as microscopic transmission ellipsometry which has been used in this thesis work. The theory of this method is described in this section. This measurement method requires using four different angles between the polarizers with at least two wavelengths of light. As microscopic transmission ellipsometry does not require invasive preparation steps, measurement of the MFA can be performed while doing e.g. a flexibility or bond strength measurement. Also, this makes the method suitable for automation.

The equipment required for applying this method is a conventional polarizing microscope equipped with a CCD (charge-coupled device) camera or microscope video camera (Fig. 2.15). In this approach, the fibre is placed between two crossed polarizers

and the light is transmitted through the fibre. The light from the light source of the microscope, with constant intensity  $I_0$ , is linearly polarized by the polarizer. The linearly polarized light sequentially passes through the two walls of the fibre to be measured.

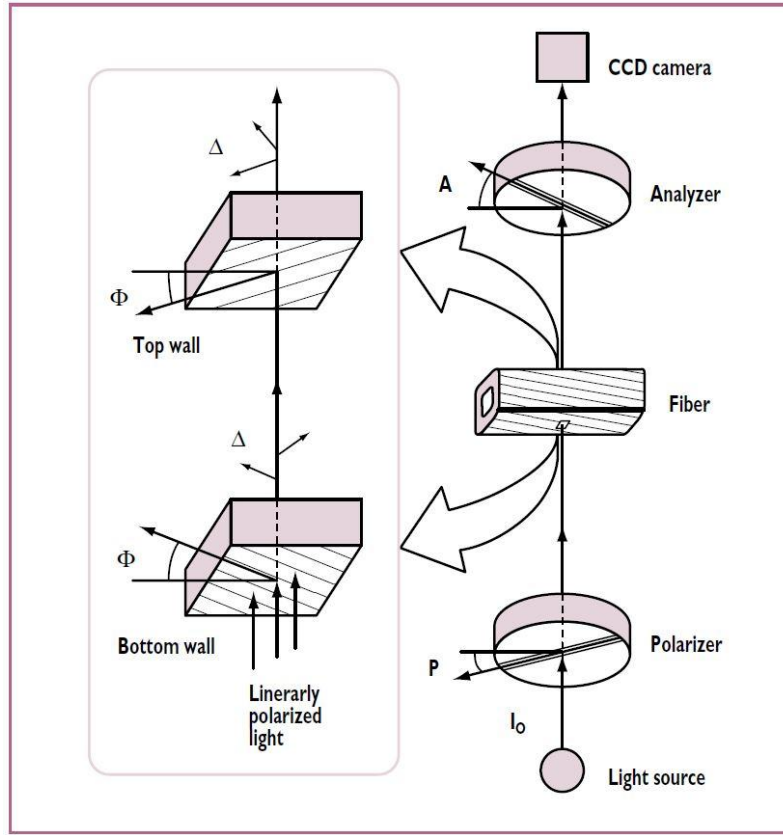


Figure 2.15 – Schematic illustration of transmission ellipsometry measurement [46]

In general, the microfibril angles of the two opposite walls of a fibre are similar but of opposite direction, and the thickness of both of the walls can be assumed to be nearly equal. The changes in brightness of the image along the fibre imply changes in MFA in the fibre wall. Moreover, it is assumed that it is possible to examine a homogenous region in the middle of the fibre, so that the influence of light scattering and refraction from the fibre wall can be ignored in practice. Measurement of the MFA is based on approximating the two fibre walls the light is passing as two linear retarders in cascade with crossed optical axes. The orientation angles of these two retarders are equal to the MFAs of the fibre walls but have opposite signs. The MFA of a single wall can be calculated from the light intensity by utilizing this two-retarder model.

According to [63], with the fibre axis as the coordinate axis and the polarizer at azimuth  $PA = 45^\circ$ , the intensity  $I(A)$  after the analyzer (azimuth  $A$ ) is as follows:

$$I(A) = \frac{I_0}{2} (1 + T_1 \cdot \sin 2A + T_2 \cdot \cos 2A) \quad (2.7)$$

Where  $I(A)$  is the intensity (0...255) of the image point at an analyzer angle  $\alpha$  degrees, and the intermediate quantities  $T_1$  and  $T_2$  for each image point are calculated with different analyzer angles.

$$T_1 = (I_{45} - I_{135}) / (I_{45} + I_{135}) \quad (2.8)$$

$$T_2 = (I_0 - I_{90}) / (I_0 + I_{90}) \quad (2.9)$$

Based on the aforementioned assumptions, the two solutions of MFA ( $\varphi$ ) for each image point are calculated [46].

$$\varphi_1 = -\frac{1}{2} \arctan\left(\frac{2T_2}{\sqrt{2+2T_1}(2-\sqrt{2+2T_1})}\right); T_1 \neq \pm 1 \quad (2.10)$$

$$\varphi_2 = \frac{1}{2} \arctan\left(\frac{2T_2}{\sqrt{2+2T_1}(2+\sqrt{2+2T_1})}\right); T_1 \neq \pm 1 \quad (2.11)$$

Only one of the results is useful, the other is just a mathematical by-product. Also, two solutions for the phase retardation for each image point are calculated [46].

$$\Delta_1 = \arccos(1 - \cos^{-2}(2\varphi_1) * \left(1 + \frac{1}{2}\sqrt{2+2T_1}\right)) \quad (2.12)$$

$$\Delta_2 = \arccos(1 - \cos^{-2}(2\varphi_2) * \left(1 - \frac{1}{2}\sqrt{2+2T_1}\right)) \quad (2.13)$$

After repeating these calculations with another wavelength, the correct value for MFA ( $\varphi_n$ ) for each image point is found when  $n$  meets these two criteria:

$$\varphi_n(\lambda_1) \approx \varphi_n(\lambda_2) \quad (2.14)$$

$$\Delta_n(\lambda_1) < \Delta_n(\lambda_2) \text{ if } \lambda_2 < \lambda_1 \quad (2.15)$$

According to the first criteria, the microfibril angle should be equal or very close for both wavelengths. In fact, the microfibril angle is not a function of wavelength and should not change when wavelength changes. Based on the second criteria, when wavelength increases, the phase retardation should decrease. This criteria is used as a cross validation for the final results.

## 2.5. Existing Functionalities of TUT's Microrobotic Platform for Fibre Characterization

TUT's microrobotic platform is developed for studies on characterization of individual pulp and paper fibres and bonds [13]. Several functionalities have been integrated to this platform during these years. The feasibility of performing multiple individual fibre and fibre bonds characterization experiments in tele-operated mode in lab scale has been demonstrated. The chief existing functionalities of the platform are described briefly in this section. As stated in the problem statement section, this thesis work aims to integrate two more functionalities to this microrobotic platform.

The first developed functionality of the platform is individual flexibility measurement [13]. The platform includes two micromanipulators for grasping, handling, and straightening of the individual fibres. In addition, the platform includes a XY-Table on top of which a capacitive force sensor is mounted. Vertical force is applied to the middle of the gripped individual fibre by the tip of the force sensor and the applied force is measured. The deflection of the fibre can be measured by the encoders of XY-Table actuators. In this method, the fibre is considered as a beam with both end fixed boundary condition under concentrated transverse loading. Hence, the flexibility of an individual fibre can be estimated according to equation 2.16.

$$Flexibility = \frac{1}{EI} = \frac{192.y}{F.L^3} \quad (2.16)$$

Where  $E$  is the Young's modulus of the fibre,  $y$  is the deflection of the fibre,  $I$  is the moment of inertia,  $F$  is the applied force, and  $L$  is the length of the fibre between two grippers. The steps of the experiment are shown in Fig 2.16.

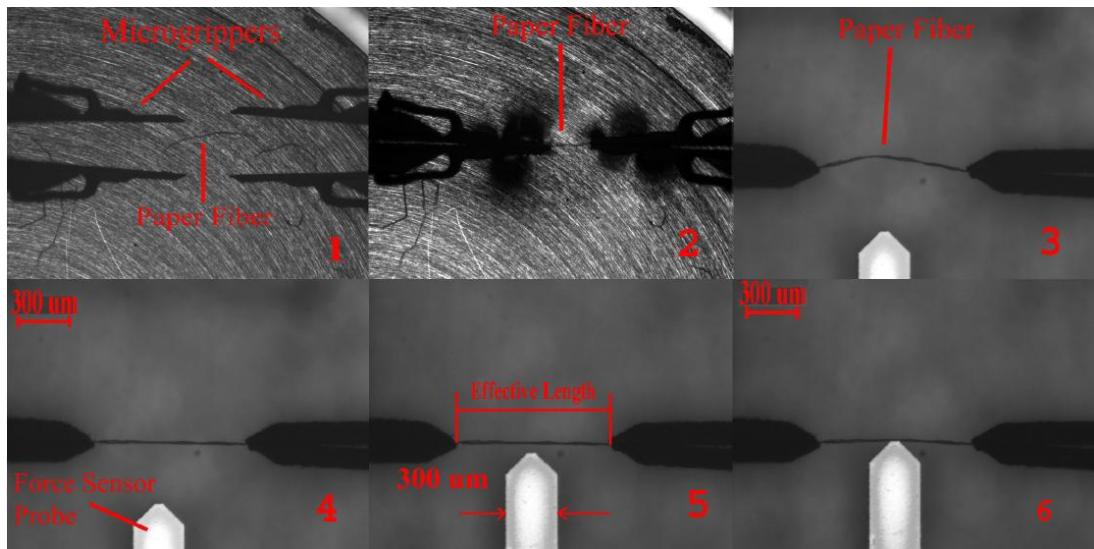


Figure 2.16 – Individual fibre flexibility measurement [13]



Making, manipulation, and breaking of individual fibre-fibre bonds is also feasible with the microrobotic platform [14]. In this method, the fibre bond is grasped from the two ends of one of the fibres using two micromanipulators. The third manipulator is used for grasping one end of the crossing fibre and pulling it until it breaks. The steps of the experiment are demonstrated in Fig 2.17.

In the next step of platform development, a force sensor is integrated to the system. Using the force sensor, individual fibre-fibre bond strength measurement has become feasible [16] [15]. The fibre bond is grasped and manipulated similar to the previous work. The force sensor is used to apply the force and breaking the bond (Fig. 2.18). Glue is used to attach the end of the fibre-fibre bond to the sensor.

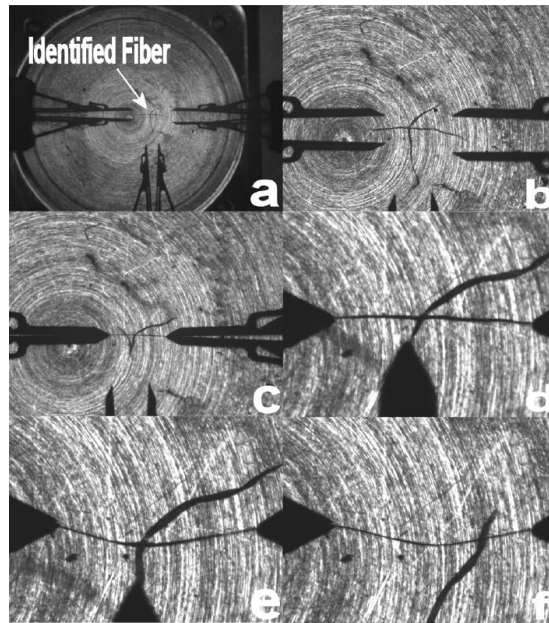


Figure 2.17 - Process of manipulating and breaking an individual fibre-fibre bond [14]



Figure 2.18 – Individual fibre-fibre bond strength measurement [15]

The platform is also capable of fibrous microscale specimens handling for various microscopic studies such as scanning electron microscopy (Fig. 2.19-a) and nanotomography (Fig. 2.19-b). Handling fibres with diameters ranging from 10 to 1000



$\mu\text{m}$  and lengths of  $100\ \mu\text{m}$ – $15\ \text{mm}$ , and mounting them on different types of specimen holders is possible with the microrobotic platform without damaging them. This minimizes human interaction with the samples. [64]

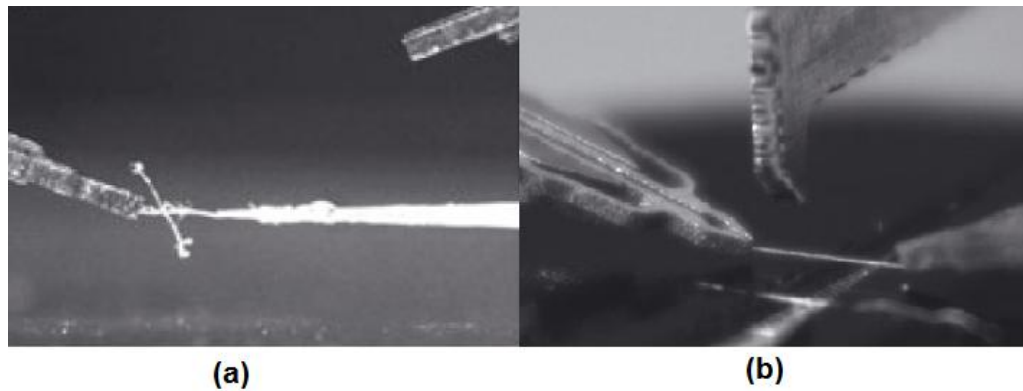


Figure 2.19 - Handling of fibre-fibre bonds for nanotomography studies (a), Fibre specimen preparation for the diagonal compression test inside an SEM (b) [64]

Another application of the microrobotic platform is evaluation of the wetting ability of individual fibres in terms of drop-on-fibre contact angle measurement [17]. In this application, a micro dispenser is integrated to the microrobotic platform for dispensing liquid droplets down to  $12\ \text{nl}$ . The microgrippers are used for grasping and handling a fibre from both ends towards the dispenser. The microgrippers straighten the fibre and align it perpendicular to the dispenser. In the next step, the probe liquid droplet is shot onto the fibre (Fig. 2.20) and the top-view vision-system starts to record a sequence of images from the droplet dynamics on the fibre. The images are analysed by an image processing code for evaluating the dynamic contact angle of the fibre. [17]

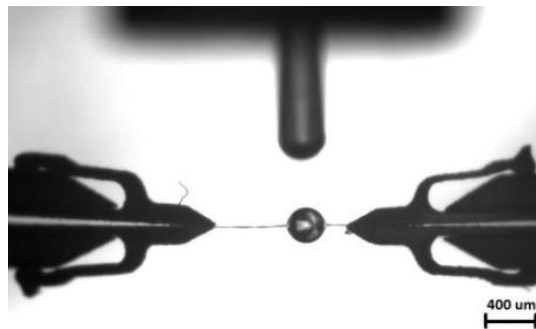


Figure 2.20 – Drop-on-fibre contact angle measurement [17]

## 2.6. T-test Analysis

T-test is one of the most widely used statistical tests which is straightforward and adaptable to a broad range of situations.

A t-test is any statistical hypothesis test in which the test statistic follows a Student's  $t$  distribution if the null hypothesis is supported. It can be used to determine if two sets of data are significantly different from each other, and is most commonly applied when the test statistic would follow a normal distribution. It often involves randomly sorting the members of a subject pool into two separate groups, treating the two groups differently with respect to a certain independent variable, and then measuring both groups on a certain dependent variable with the aim of determining whether the differential treatment produces differential effects.

In each of these cases, the two samples are independent of each other in the obvious sense that they are separate samples containing different sets of individual subjects. The individual measures in group A are in no way linked with or related to any of the individual measures in group B, and vice versa. The version of a t-test examined in this section will assess the significance of the difference between the means of two such samples.

These steps should be done to perform an Unpaired T-test to the sample data:

Step 1. For the two samples, A and B, of sizes of  $N_a$  and  $N_b$  respectively, the mean ( $MX_a$  and  $MX_b$ ) and sum of squared deviates of samples ( $SS_a$  and  $SS_b$ ) are calculated.

Step 2. The variance of the population of measures that the null hypothesis assumes to have been the common source of the measures in both groups is estimated based on equation below:

$$s^2 = \frac{SS_a + SS_b}{(N_a - 1) + (N_b - 1)} \quad (2.12)$$

Step 3. The standard deviation of the sampling distribution of sample-mean differences is calculated based on equation below:

$$\sigma_{M-M} = \sqrt{\frac{s^2}{N_a} + \frac{s^2}{N_b}} \quad (2.13)$$

Step 4. In this step the parameter  $t$  is calculated based on the equation below. Greater the parameter  $t$ , more the level of significance between the samples is.

$$t = \frac{MX_a - MX_b}{\sigma_{M-M}} \quad (2.14)$$

Step 5.  $P$  value is calculated based on Table 2.2. Lower the  $P$  value, more the level of significance between the samples is. These levels are estimated based on  $t$  and  $df$  which

is calculated through below equation. The parameter  $df$  is an index shows how massive the samples are.

$$df = (N_a - 1) + (N_b - 1) \quad (2.15)$$

Table 2.2 – Level of significance versus  $df$  and  $t$

	Level of Significance				
<b>df</b>	<b>0.10</b>	<b>0.05</b>	<b>0.02</b>	<b>0.01</b>	<b>0.001</b>
<b>1</b>	6.31	12.71	31.82	63.66	636.58
<b>2</b>	2.92	4.30	6.96	9.92	31.60
<b>3</b>	2.35	3.18	4.54	5.84	12.92
<b>4</b>	2.13	2.78	3.75	4.60	8.61
<b>5</b>	2.02	2.57	3.36	4.03	6.87
<b>6</b>	1.94	2.45	3.14	3.71	5.96
<b>7</b>	1.89	2.36	3.00	3.50	5.41
<b>8</b>	1.86	2.31	2.90	3.36	5.04
<b>9</b>	1.83	2.26	2.82	3.25	4.78
<b>10</b>	1.81	2.23	2.76	3.17	4.59
<b>11</b>	1.80	2.20	2.72	3.11	4.44

Step 6. The probability of rejection of null hypothesis is then calculated based on equation below.

$$Probability = (1 - P) * 100 \quad (2.16)$$

## 2.7. Discussion

A general overview of micromanipulation systems has been given. Components of micromanipulation systems and possible areas of application have been presented. Microforce sensing methods and pros and cons of each method are explained briefly in this chapter. In this thesis work, a PVDF film is used as the microforce sensing element. The PVDF film provides a surface to integrate the needed components for the measurement. Moreover, it can be easily integrated to a micromanipulation system. Due to high sensitivity of piezo-based microforce sensors, small changes in the applied force can be detected which is highly required in individual fibre-fibre bond strength measurement.

The morphological and mechanical paper fibre properties have been generally introduced. Z-directional fibre-fibre bond strength has been defined, and different experimental evaluation methods of Z-directional strength are described and pros and cons of each are explained. As discussed, there is a high demand in paper research and

industry for measurement of Z-directional bond strength at a single fibre level. However, there is not any method to address this need. Indeed, development of a method for measurement of Z-directional individual fibre-fibre bond strength is beyond state-of-the-art measurement methods.

Furthermore, the definition, importance, and current measurement methods of microfibril angle are described. In this thesis work, transmission ellipsometry method is selected for microfibril angle measurement. Using this method, sample pre-treatment is not needed, and there is high capability in the method for automated measurements. As the most significant upside of this method, the measurement components can be integrated to a micromanipulation system which provides the possibility of microfibril angle measurement during mechanical characterization of individual fibres and fibre bonds. The theory of the implemented microfibril angle measurement method has been described in this chapter.

Existing functionalities of TUT's microrobotic platform including flexibility measurement, bond manipulation and breaking, bond strength measurement, contact angle measurement, and sample preparation for microscopy applications have been also explained. T-test analysis is also briefly described in this chapter.

### 3. Research Methods and Materials

The purpose of this chapter is to provide the required information on the research methods and materials used in this thesis work. As stated in problem statement part, this research work aims to develop experimental methods for measuring Z-directional fibre-fibre bond strength and microfibril angle. Microrobotics is used as the method due to different reasons. The chief reason is the high potential of microrobotics for automation which facilitates high throughput measurements. Furthermore, the human interaction with the fibre samples is decreased using micromanipulators for handling and manipulating the fibres and fibre bonds. Moreover, microrobotics facilitates multiple unique functionalities in fibre characterization which are explained in details in this section. These features distinguish microrobotics from the other measurement methods discussed in the previous chapter.

In this chapter, a general overview of the microrobotic platforms used in this research is given. Then, the conceptual design of the Z-directional fibre-fibre bond strength measurement is explained. The calibration procedure of the microforce sensor is described, and the results of calibration for different deformation rates are presented. Next, the proposed protocol for Z-directional fibre-fibre bond strength is explained in details. Afterwards, the conceptual design and implementation of the microfibril angle measurement system is described. Finally, the microfibril angle measurement protocol is presented.

#### 3.1. Overview of the Microrobotic Platforms

TUT's microrobotic platforms have been used as the framework in this research. Microrobotic Platform A (Fig. 3.1) is a multi-purpose device for fibre characterization studies [13]. The main functionalities of this platform are explained briefly in chapter 2. Fibre manipulation and experiments are performed in a tele-operated framework. The Z-directional bond strength functionality is integrated to this platform. The platform includes three micromanipulators (SmarAct Co., Germany) with four degrees of freedom (DOF) constructed from three linear micropositioners and a microgripper to grasp and manipulate the individual fibre-fibre bond (IFFB) in the XYZ directions. The movement of the micromanipulators can be also synchronized. A 1DOF rotary table (SmarAct GmbH., Germany) are mounted on the top of a 2DOF XY-table (SmarAct

GmbH., Germany). The rotary table is used to orient the IFFBs. Additional components can be integrated to the platform for certain experiments such as microforce sensor, microdispensor, etc. A Sony-XCDU100 camera (Sony Co., Japan) and a motorized 12X Zoom with 3.5X magnification (Navitar, USA) are used to image the side view, and a Manta-G504 camera (AVT AG, Germany) is used to image the front view of the platform.

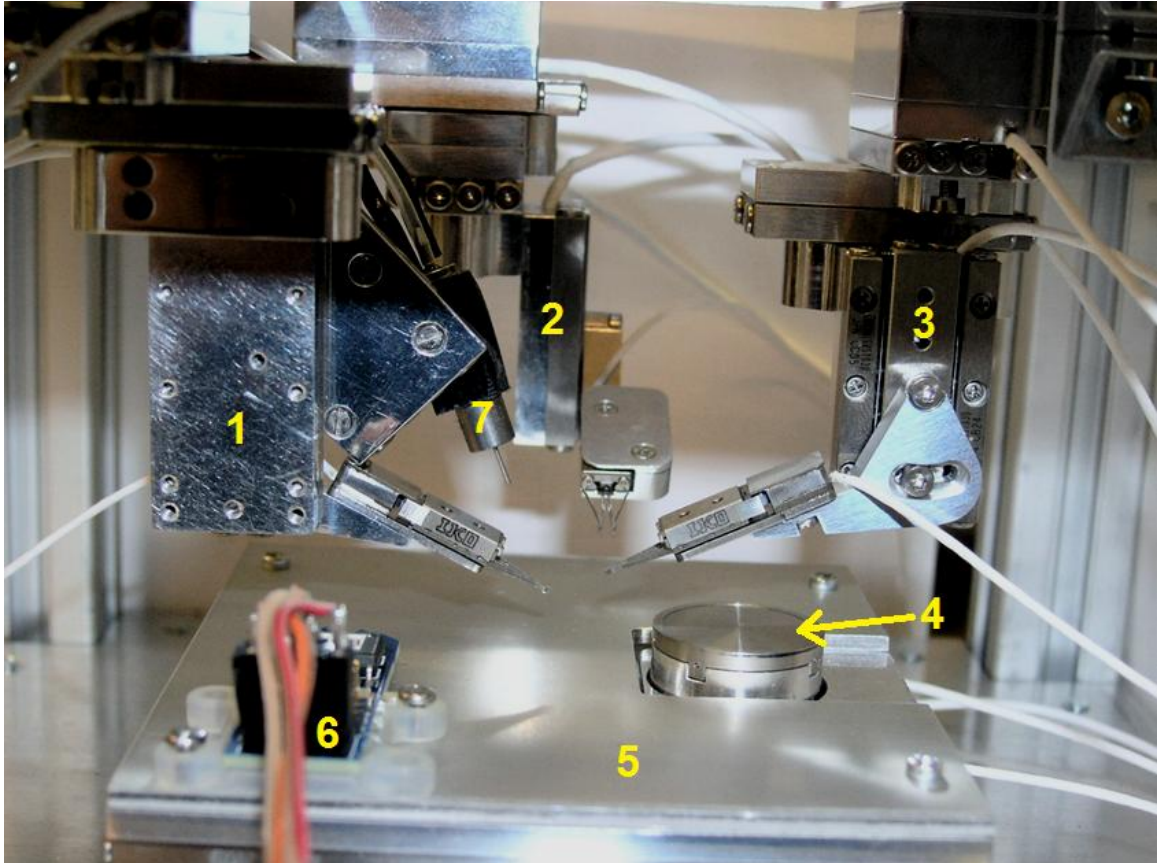


Figure 3.1 - Implementation of Microrobotic Platform A: 1, 2, and 3) XYZ-micromanipulators; 4) Rotary table; 5) XY-table; 6) Microforce sensor; 7) Microdispensor. [13]

Microrobotic Platform B is designed for future automated and autonomous micromanipulation and characterization of fibres. Mechanical design and fabrication of the mechanical components of this system has been a part of this thesis work. The Microrobotic Platform B is modelled with CATIA V5 (Fig. 3.2). The chief differences of this platform and the Microrobotic Platform A are in visualization i.e. the illumination and imaging systems. The imaging system consists of two cameras, equipped with motorized optics and polarizers. The cameras are located above the micromanipulators. The angle between the cameras is  $30^\circ$ . The illumination system is designed to acquire high-contrast images of fibres, a backlight, a polarizer and an analyzer were used in imaging. When there is a  $90^\circ$  phase difference between the polarizer and the analyzer, the polarizer blocks all the light that does not pass the fibres

and thus change its polarity. The polarizer and the backlight elements are located inside of a sample holder so that it remains stationary while the samples are rotated during the alignment. The illumination system design is explained in details in [65]. This configuration facilitates 3D reconstruction of the fibres from 2D images which is explained in details in [66]. Microrobotic Platform B consists of three 4-DOF and one 3-DOF manipulators that are assembled in a stacked gantry crane configuration. The 4-DOF manipulators are constructed from three linear micropositioners and a microgripper (SLC- 1740, SG-1730-M, SmarAct GmbH) which are used for grasping and micromanipulation of the fibres. The 3-DOF manipulator consists of two linear and one rotary micropositioners (SLC- 1760, SR-4513-S, SmarAct GmbH). The samples are initially placed on a circular glass slide that resides on top of sample holder. The components for microfibril angle measurement are integrated to this Microrobotic Platform. The fabricated Microrobotic Platform is illustrated in Fig. 3.3.

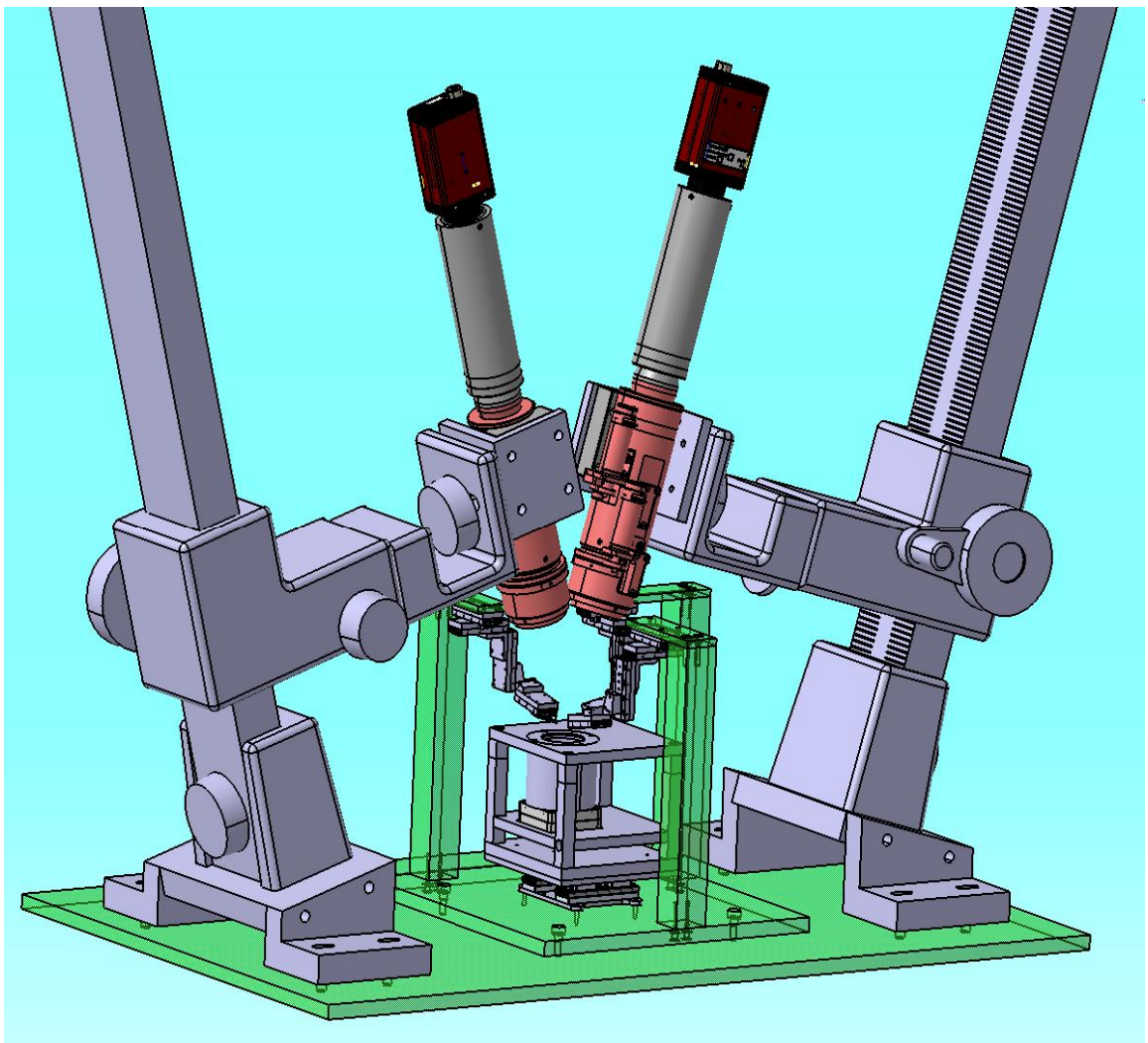


Figure 3.2 – 3D model of Microrobotic Platform B



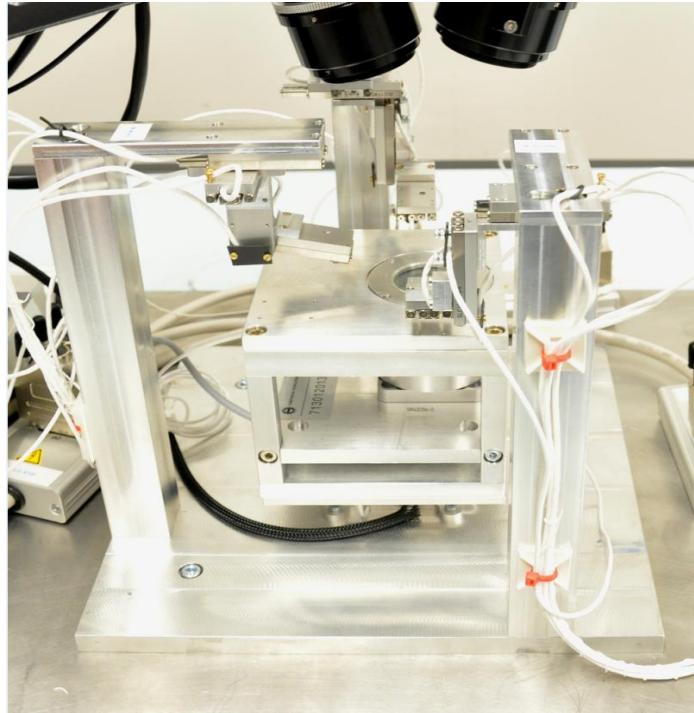


Figure 3.3 – Photograph of Microrobotic Platform B

### 3.2. Z-Directional Individual Fibre-Fibre Bond Strength Measurement Method

This thesis work presents the first ever developed Z-directional fibre-fibre bond strength measurement method at the fibre level. First, the conceptual design of the method is described. Afterwards, the microforce sensing system design and calibration procedure are explained. The calibration of the microforce sensing system for multiple deformation rates of PVDF sensor is performed and the results are also presented in this section. Finally, the protocol for Z-directional fibre-fibre bond strength measurement is presented.

#### 3.2.1. Conceptual Design

In general, the first step of system design is requirement specification which sets out the specifications that the system is expected to provide. In this Section, the principal requirements of the Z-directional IFFB strength measurement method are identified and listed as follows.

1. Sample storage is required to sort and store the dry IFFBs. It should be noted that the IFFB making process is assumed separately from the measurement method.
2. Micro-positioning of the IFFBs in XY directions is needed. The XY working area should be approximately 30 mm \* 30 mm.
3. Micro-orienting of the IFFBs should be facilitated so that IFFB grasping becomes feasible from all ends of the IFFBs.



4. Micro-gripping of the IFFBs is needed. Two 3-DOF micromanipulators are required for manipulation of the IFFBs in XYZ directions. The microgrippers should be integrated to the micromanipulators to grasp the IFFBs. The XYZ working area of micromanipulators should be approximately 30 mm \* 30 mm \* 30 mm. There should be a common working area of 20 mm \* 20 mm \* 30 mm for the micromanipulators.
5. Two free ends of one fibre of IFFB should be fixed. The ends of the other fibre should be moved synchronously to the Z-direction of the IFFB until the IFFB breaks.
6. A microforce sensor is required to measure the Z-directional force from starting the force application to the IFFB until IFFB breaking. The force range of the microforce sensor should be approximately 1-20 mN.
7. The imaging of the measurement should be facilitated from the Z-direction of the bond (Top View), and parallel with the bond plane (Side View).
8. Zooming, focusing, and illumination should be facilitated so that an IFFB is visualized in the highest level of zoom in both imaging directions. The whole working area of the XYZ micromanipulators should be visible in the lowest level of zoom.
9. A control system is needed to facilitate tele-operated micromanipulation of the IFFBs. The control system should enable visualization control e.g. focusing, zooming, and illumination control as well.

To address these requirements, a measurement system is conceptually designed. The conceptual design of the measurement method and the main functions are illustrated in Fig. 3.4. The main functions are Micromanipulation (F1), Visualization (F2), Sample Storage (F3), Control (F4), and Microforce Sensing (F5).

Micromanipulation function (F1) enables micropositioning, micro-orienting and microgripping of the IFFBs. This function is used for placing the IFFB, the rotary table, the sensing element in the working space of microgrippers. It also facilitates the change of IFFB orientation. Moreover, grasping and handling of IFFBs is performed with this function.

Visualization function (F2) facilitates imaging, magnification, illumination and signal analysis. The visual information is used as visual feedback in the control function (F4).

Sample storage function (F3) facilitates the IFFBs storage. The IFFBs are prepared separately and stored via this function.

The Control function (F4) enables the micromanipulation control which controls micropositioning, micro-orienting and microgripping devices. Visualization control including zooming and fine focusing is also performed with this function. A user interface connects all the control sub-functions to the human operator.

Microforce sensing function (F5) enables the measurement of the force magnitude required to break an IFFB.

Micromanipulation, visualization, sample storage, and control functions are already available in Microrobotic Platform A. Microforce sensing function should be designed based on the stated requirements and integrated to the Microrobotic Platform A to facilitate the measurement. The design and implementation of the microforce sensing system is described in details in the next section.

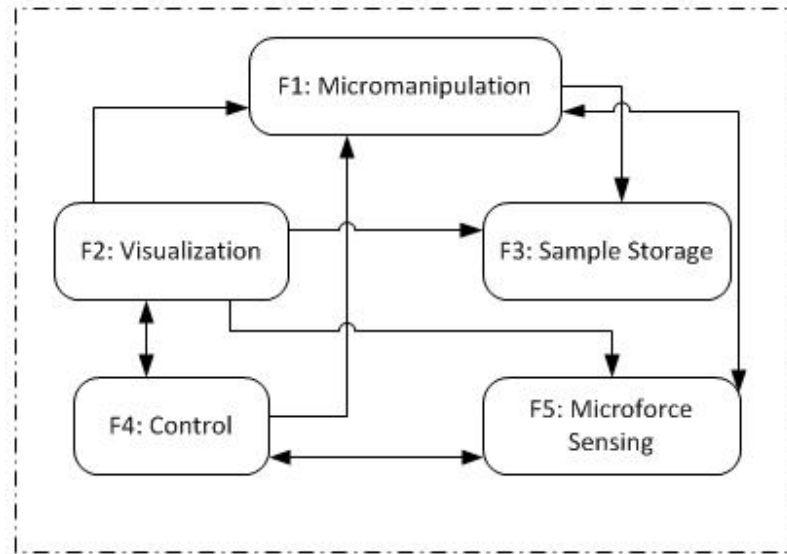


Figure 3.4 - Conceptual design of the method for Z-directional strength measurement of IFFBs

### 3.2.2. Microforce Sensing System Design and Implementation

A schematic design of the microforce sensing system is illustrated in Fig. 3.5. The module is composed of four elements which are described in this section. When a Z-directional force is applied to the bond, this force is transferred to the PVDF film element via connecting parts and bends the film. Based on piezoelectric effect, an internal electric charge is generated in the PVDF film. The generated internal electric charge is a function of the applied force magnitude [40]. The main elements of the sensor are as follows.

1. A piezoelectric PVDF polymer film [40] which is used as the main sensing component (Item 2 in Fig. 3.5).
2. The bond holder which is used for bond mounting (Item 4 in Fig. 3.5).
3. The connecting element which is used to connect the bond holder to the sensing element. This element should be fixed on the sensing element (Item 3 in Fig. 3.5).
4. The mounting stage on which the sensing element is fixed and connected to the microrobotic platform (Item 5 in Fig. 3.5).

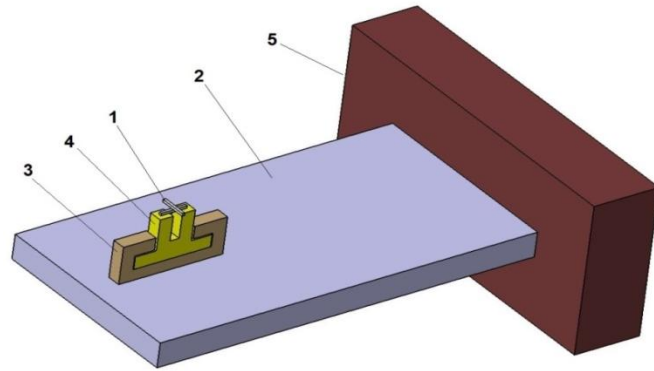


Figure 3.5 - Schematic design of the force sensing module: 1) IFFB; 2) piezoelectric PVDF polymer film; 3) Connecting element; 4) Bond holder; 5) Mounting stage. [40]

The implementation of the sensing system is illustrated in Fig. 3.6. The PVDF element (LDT0-028K model, Measurement Specialties Inc., USA) is made of a 28  $\mu\text{m}$  thick piezoelectric PVDF polymer film with screen-printed Ag-ink electrodes and laminated to a 0.125 mm polyester substrate. The connecting element and the bond holder are fabricated using 3D-printing fabrication method (miniFactory Oy Ltd., Finland). The used material is white PLA (Poly Lactic Acid). Since the 3D-printer nozzle diameter is 300  $\mu\text{m}$ , the extruded path is manually designed to assure that the printed layers are continuous and without conflict. This enhanced the quality of the fabricated parts. The parts have ten 0.08 mm thick layers which are printed on top of each other.

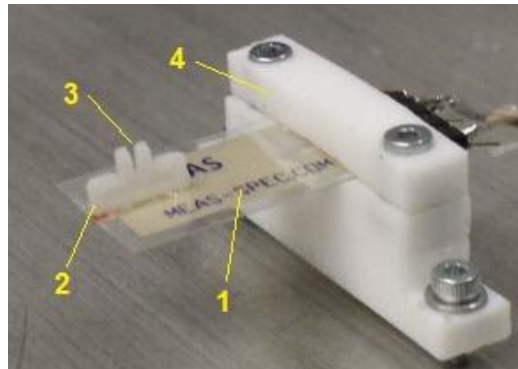


Figure 3.6 - Implementation of the Sensor: 1) PVDF film; 2) Connecting element; 3) Bond holder; 4) Mounting stage. [40]

The connecting element is mounted and fixed on the PVDF film using glue permanently (Fig. 3.7-A). The bond holder is a removable piece (Fig. 3.7-B) which is a consumable part for each experiment. However, the bond holder can be cleaned using acetone and reused in the experiments if needed. Super glue is used to attach the free ends of the IFFB to the bond holder. A stack for bond holders (Fig. 3.7-C) is fabricated using milling. Nine different bond holders can be placed on the stack during sample

preparation procedure which enhances the speed of sample preparation. The mounting stage is fabricated using drilling and milling to mount and fix the sensing element on the XY table of the microrobotic platform.

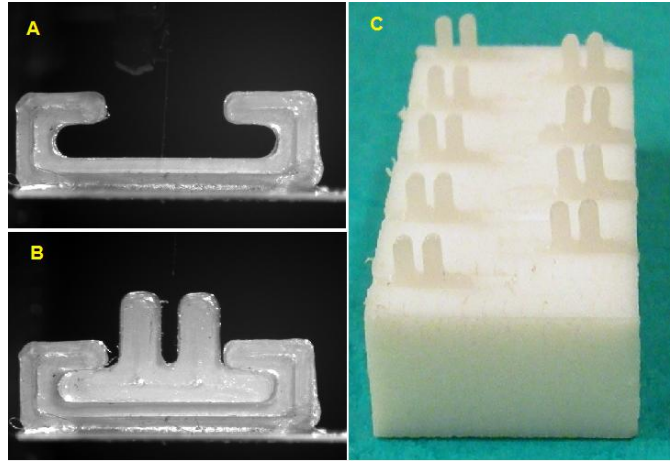


Figure 3.7 - A) Connecting element; B) Bond holder placed inside the Connecting element; C) Stack of Bond holders. [40]

The sensing module is integrated to the first Microrobotic Platform A. Fig. 3.8 illustrates the implementation and configuration of the microrobotic platform for Z-directional fibre-fibre bond strength measurement.

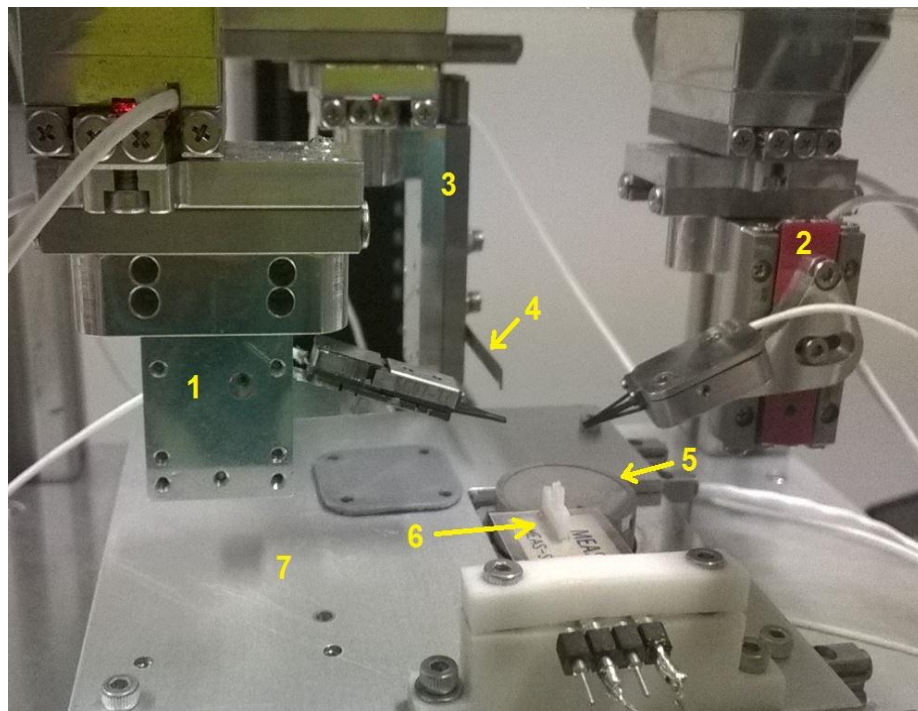


Figure 3.8 - Implementation of the microrobotic platform. 1) and 2) XYZ-microgrippers, 3) L-shaped-micromanipulator, 4) L-shaped probe, 5) Rotary table, 6) Sensing module, 7) XY-table.

### 3.2.3. Microforce Sensing System Calibration

Calibration is an essential process before proper application of a microforce sensor. Calibration is a procedure for mapping the correspondence between the output signal of a force sensor -which is usually a voltage or current signal- and a known force. In calibration process, a known force is applied to the sensor, which produces a corresponding output signal. A number of known forces in the load range of microforce sensor are applied to the microforce sensor, and the output signals are recorded. In the next step, a linear interpolation is performed between zero load and the known maximum load. The resulted curve is called calibration curve which determines the actual force range that matches the sensor output range. In this section, the calibration procedure which has been performed to calibrate the PVDF microforce sensor is explained.

The calibration setup design is explained in details in [40]. For calibration of the PVDF microforce sensor, a capacitive microforce sensor (FT-S10000, FemtoTools AG, Switzerland) is used as a reference sensor which is shown in Fig. 3.9. Both compression and tension forces can be measured. A tensile force will result in an increase of the output voltage whereas a compression force will result in a decrease of the output voltage. The force measurement range, the sensitivity, and the resolution of the FT-S10000 sensor are  $\pm 10,000 \mu\text{N}$ ,  $5000 \mu\text{N/V}$ , and  $5 \mu\text{N}$ , respectively.



Figure 3.9 – Reference microforce sensor

The design of the calibration setup is discussed in details in [40]. For the calibration of the sensor, the PVDF microforce sensor is mounted on top of the XY table. The FT-S10000 sensor is attached to an SLC-1730 actuator (Smaract GmbH, Germany) by means of an L-shaped connector so that the movement of the FT-S10000 sensor can be controlled with the actuator movement. The accuracy, repeatability, and the resolution of the SLC-1730 actuator are  $1 \mu\text{m/m}$ ,  $30 \text{ nm}$ , and  $1 \text{ nm}$ , respectively. The FT-S10000 sensor is positioned so that the tip of the sensor is perpendicular to the desired sensing point of the PVDF microforce sensor. The configuration of the calibration setup is shown in Fig 3.10.

Two cameras are used to image the calibration setup during calibration process. A Sony-XCDU100 camera (Sony Co., Japan) and a motorized 12X Zoom with 3.5X magnification (Navitar, USA) are used to image the side view, and a Manta-G504 camera (AVT AG, Germany) is used to image the front view of the calibration setup. To



start the calibration loading cycle, the connecting element of the PVDF microforce sensor should be perpendicular and in contact with the tip of the reference sensor. The side view camera is used to control the Perpendicularity. To find the contact point, the output signal of the reference force sensor is checked. When the signal starts rising, the position of the reference sensor is set as the zero contact level, and is considered as the zero load. The zero load position (contact point) and the full range load position are illustrated in Fig 3.11.

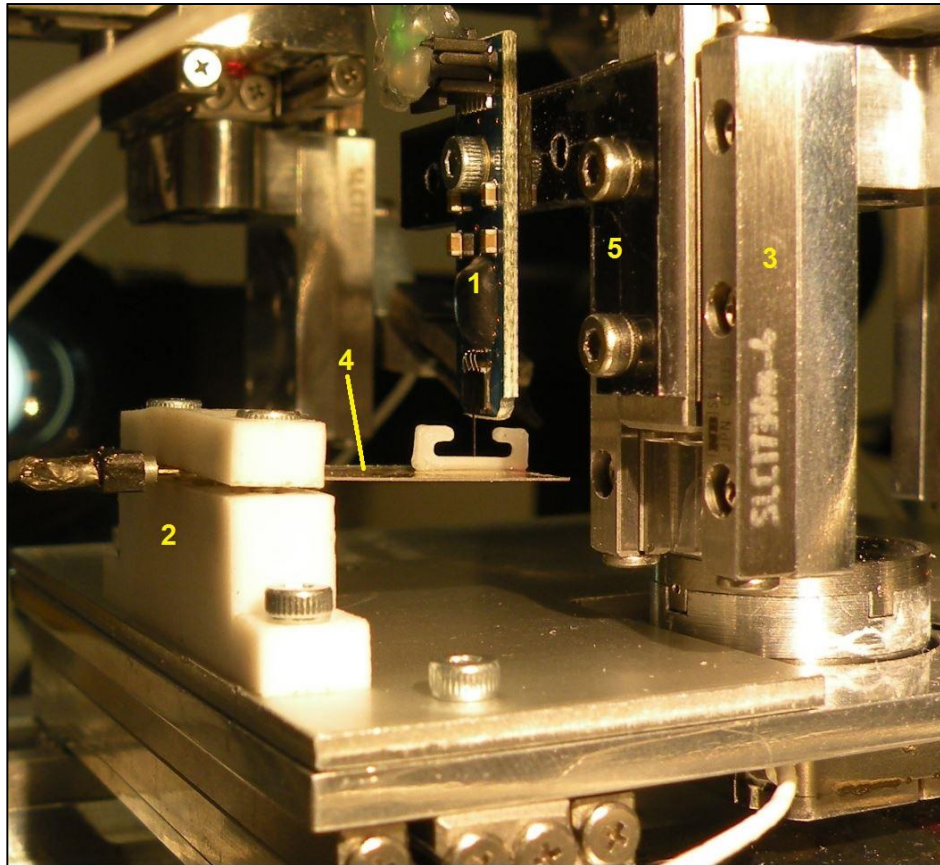


Figure 3.10 – Implementation of the calibration setup: 1) FT-S10000 sensor (reference sensor); 2) PVDF microforce sensing module; 3) SLC-1730 actuator; 4) PVDF film; 5) L-shaped connector. [40]

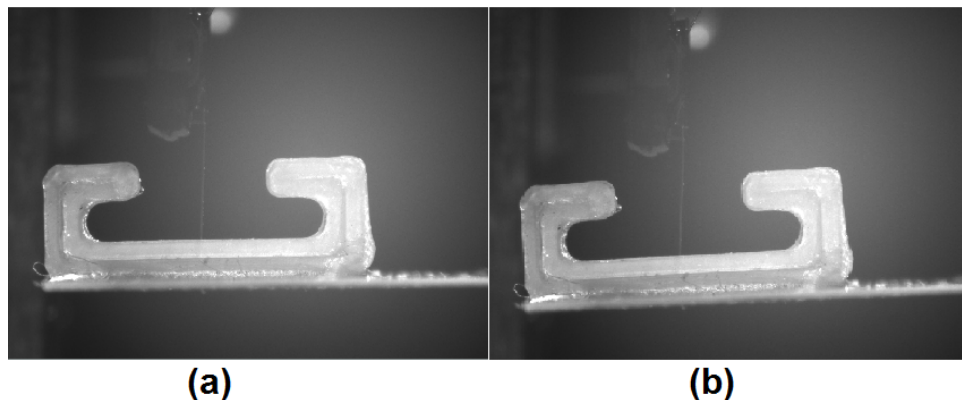


Figure 3.11 – Load application for calibration: a) zero load; b) full range load.

The linear actuator is controlled using a computer through an SCU controller (Smaract GmbH, Germany). A series of nine square pulses of from 50  $\mu\text{m}$  to 450  $\mu\text{m}$  with steps of 50  $\mu\text{m}$  is used for calibrating the sensor. Since the reference sensor is a capacitive sensor with capacitance measurement working principle, to enhance the level of accuracy in the calibration procedure, the actuator should return to its initial position (zero load level) after each step input. The waiting time for each step input is 3 seconds. In order to perform the calibration experiment, the input signal is repeated ten times. During the loading of the PVDF film, the linear actuator is moved forward and the force in the reference sensor increases, which causes the PVDF film to bend down. The deformation in the PVDF film results in a voltage change in its output. The output force of the reference force sensor for the described loading cycle, and the corresponding output voltage of the PVDF film sensor are recorded. The input loading cycle of the calibration process is presented in Fig 3.12.

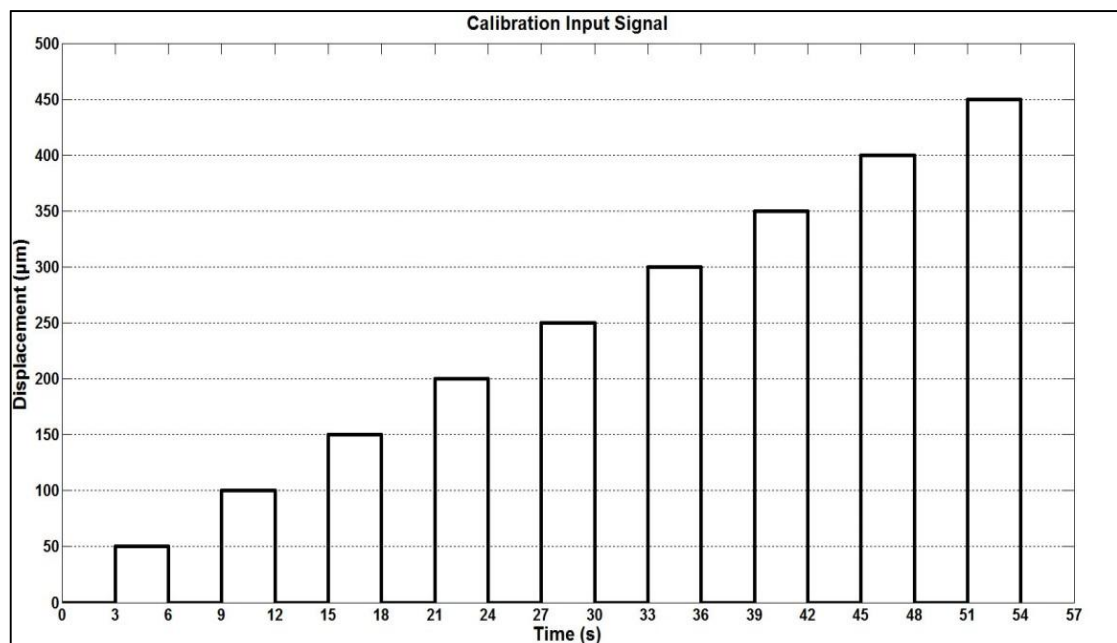


Figure 3.12 - Input signal sequence for PVDF microforce sensor calibration [40]

The reference force sensor output vs displacement for the aforementioned loading cycle is presented in Fig. 3.13. The output of the reference sensor is increasing linearly in every cycle and there is a small deviation between each cycle. The voltage difference in the output of PVDF microforce sensor for the same experiment is shown in Fig. 3.14. It is illustrated that the voltage difference in the output of the PVDF film increases linearly in every cycle, and there is a small deviation between each cycle.

As the tip of the FT-S10000 sensor (reference sensor) has been in mechanical contact with the PVDF microforce sensor connecting element, the displacement of the sensors is assumed equal. Thus, the calibration curve is plotted which is the reference force sensor output vs the voltage output of the PVDF microforce sensor. The calibration curve is shown in Fig. 3.15. The more detailed analysis of the results is presented in [40].

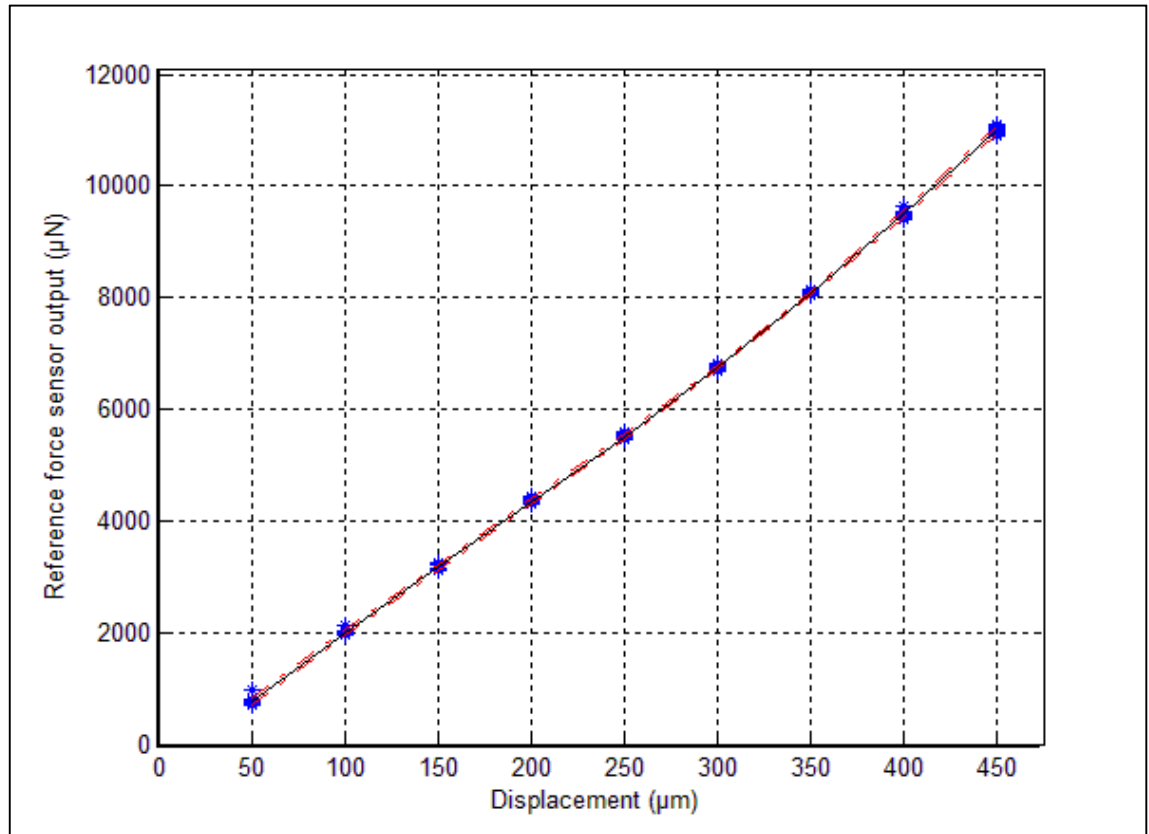


Figure 3.13 – FT-S10000 sensor (reference force sensor) output vs actuator displacement

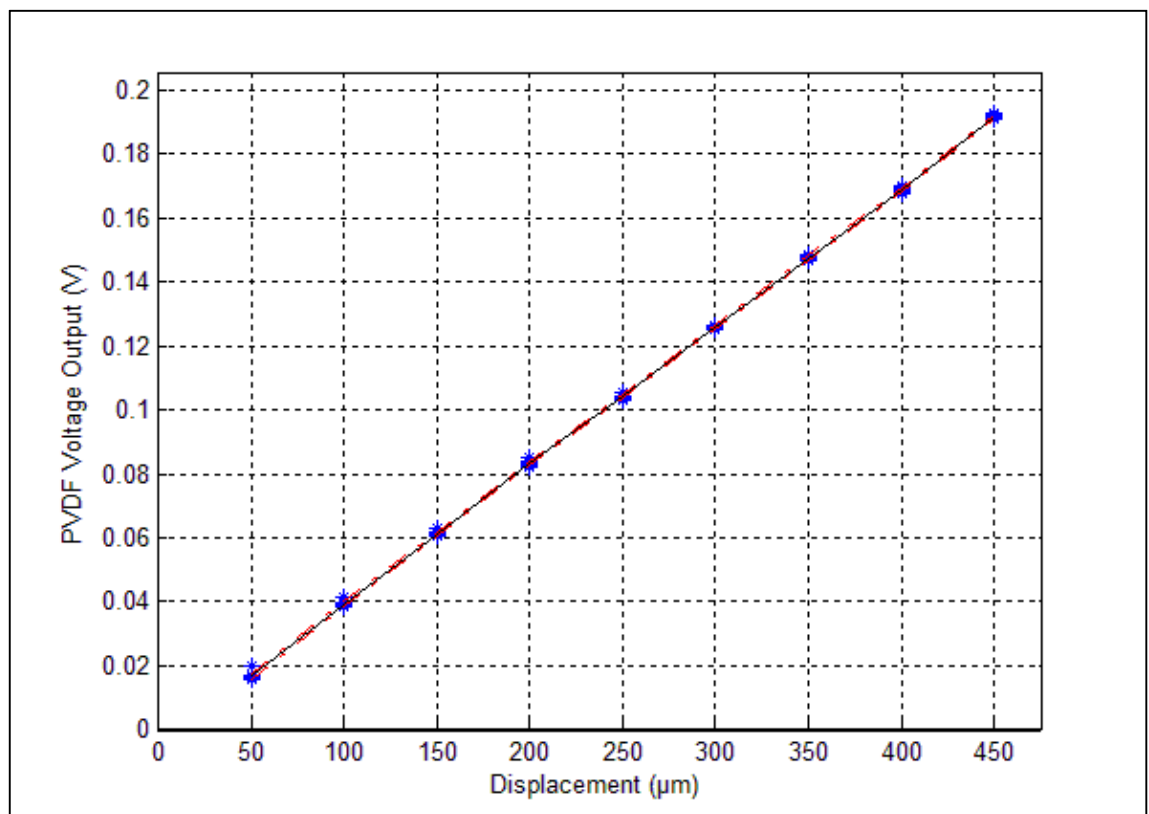


Figure 3.14 – PVDF microforce voltage output vs actuator displacement



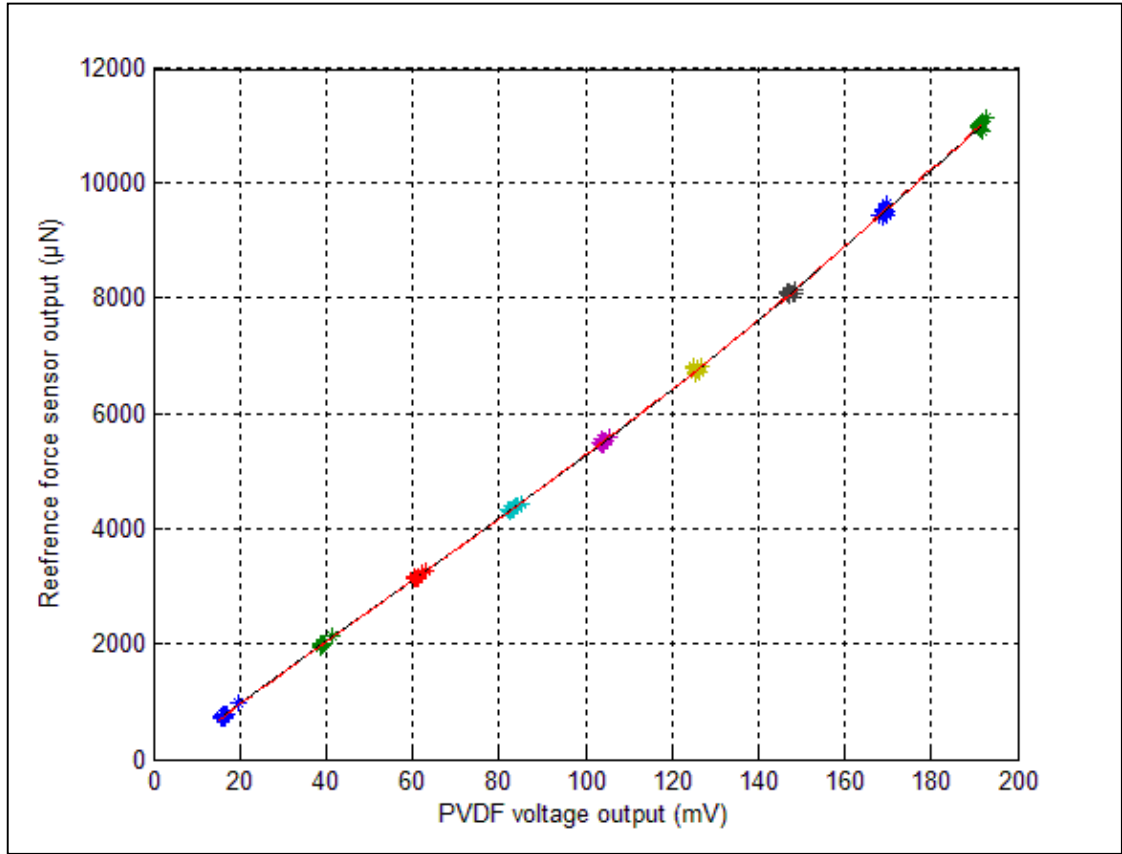


Figure 3.15 – Linear calibration curve of the PVDF microforce sensor

The equation for the calibration curve is linear and has the following form:

$$FZ = P_1 * \Delta v + P_2 \quad (3.1)$$

Where,  $FZ$  is the Z-directional force,  $\Delta v$  is the output voltage of the PVDF sensor,  $P_1$  and  $P_2$  are the slope and offset of the fitted line, respectively.

The PVDF film sensor developed in [40] is a dynamic force measurement sensor, and the response of the sensor is dependent to the deformation rate of the sensor. As it is essential in tensile testing studies to analyse different deformation rates, the effect of the deformation rate on the PVDF sensor performance is experimentally studied. It is required to validate if different calibrations are needed for different deformation rates. Different deformation rates are studied by changing the actuation frequency of the linear actuator and thus the loading velocity.

To extract the linear velocity of the microactuator which is assumed as the deformation rate of the sensor, the microactuator is moved with the same cycle shown in Fig. 3.12. The displacement of the microactuator is read using a magnetic encoder. Using the time-displacement curves of the actuator and the fact that the velocity is the first derivative of displacement, the average velocity of the actuator for each actuation frequency is extracted.

The calibration setup and procedure of the PVDF film microforce sensor are explained in the previous section. This calibration procedure has been performed for different deformation rates of the sensor. The calibration parameters ( $P_1$  and  $P_2$ ) are obtained for different deformation rates. The results are presented in the results chapter of the thesis.

### 3.2.4. Individual Fibre-Fibre Bond Making

The first step of the Z-directional individual fibre-fibre bond strength measurement is fabricating the bonds. There are two methods to fabricate the bonds. The first method is performed by means of star-shaped bond holders and micro cross parts which is described in details in [15]. In this study, the second method is used to fabricate the bonds in which a highly dilute suspension of fibres is placed between two Teflon plates and dried for 45 minutes in 70 °C under 140 kN/m<sup>2</sup> pressure. To prepare the suspension, 0,03 g of pulp fibres are suspended in 40 ml deionized water. If the mass of the paper fibres is increased there will be too many fibres on the Teflon plate and they will end up in clusters or simply overlap each other. If we use less, the number of fibres is too small and there are small chances of getting the bond samples. Since the fibre samples are white, the colour of the Teflon plates is decided to be black to get the best contrast. The droplets of suspension are positioned on the Teflon plates in rows of 3-4 droplets so that they are approximately 1 cm away from the edge of the plate and from each other in a matrix structure (Fig. 3.16 - a).

In the next step the plates are stacked and pressed with a mass. The mass should be calculated based on the area of the Teflon plates to provide the aforementioned pressure. The stack of the Teflon plates is shown in Fig. 3.16 - b.

After the droplets are positioned on to the Teflon plates and after the plates are stacked and pressed with the weight on top of them, they need to be dried. This is done with an oven at 70°C for 45 minutes time.

In the next step, the Teflon plate is placed under a light microscope to identify the IFFBs; the IFFBs are moved from the Teflon plate to the rotary table using a tweezers.

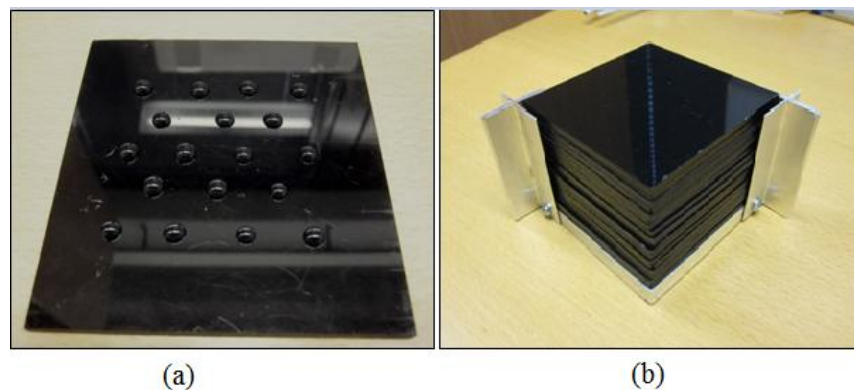


Figure 3.16 – Positioning of the droplets on the plates (a) - Stack of bond holders (b)

### 3.2.5. Z-Directional Bond Strength Measurement Protocol

The Z-directional fibre-fibre bond strength measurement is performed in a tele-operated process using the aforementioned microrobotic platform. The XY-table moves the rotary table under the field-of-view (FOV). After orienting the IFFBs using the rotary table, the overlapping area is imaged to later measure the visible overlapping area. After imaging the overlapping area of the IFFBs, one of the IFFBs is grasped and picked-up with two synchronously moving microgrippers.

The stack of the bond holders is placed on the microrobotic platform, which is used to mount the fibre bonds on the bond holders. The IFFB is grasped using a microgripper attached to a XYZ-micromanipulator. The grasped IFFB is then manipulated to the proximity of the bond holder. IFFB manipulation close the bond holder is illustrated in Fig. 3.17 - a.

In the next step, IFFB is positioned and mounted on the bond holder. A Cyanoacrylate adhesive is added to one side of the bond holder using syringe. One end of a fibre in the IFFB is then placed inside the glue. IFFB is moved in small steps using the microgripper to assure that the IFFB is fixed properly on the bond holder. Afterwards, super glue is added to the other side of the bond holder. The microgripper releases the IFFB, and a passive probe which is attached to an XYZ-micromanipulator places the other end of the fibre bond in the glue. This is illustrated in Fig. 3.17 - b.

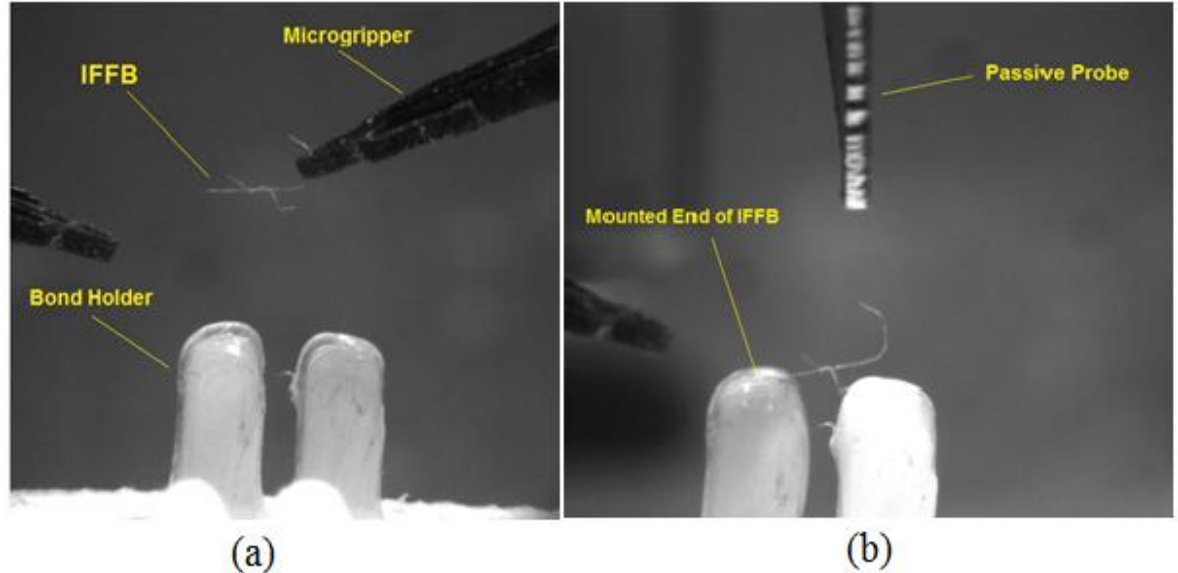


Figure 3.17 - IFFB manipulation near the bond holder (a) - IFFB mounting on the bond holder (b)

A mounted IFFB on the bond holder is shown in Fig. 3.18. In the next step, the bond holder is placed inside the connecting element of the sensing module using tweezers, and the sensing module is mounted and fixed on the XY-Table of the microrobotic platform using two screws on the mounting stage. A Z-directional force is applied to the

IFFB to break the bond by grasping both free ends of the fibre bond using two microgrippers and moving them synchronously in the Z-direction until the bond breaks. The fibre experiments in this paper were done using  $4579 \mu\text{m}/\text{sec}$ , i.e.  $15000 \text{ Hz}$  actuation frequency. Z-directional force application is illustrated in Fig. 3.19.

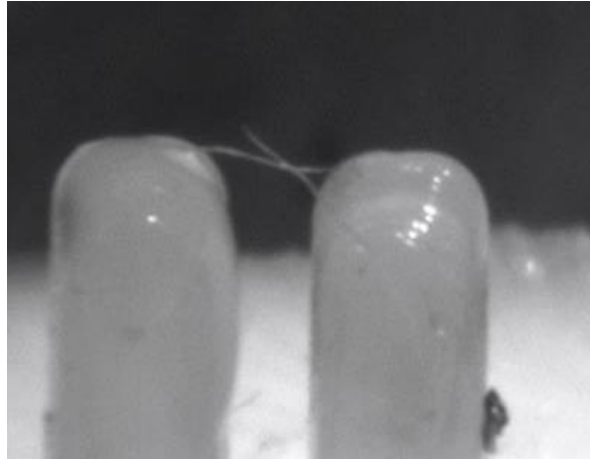


Figure 3.18 - Mounted IFFB

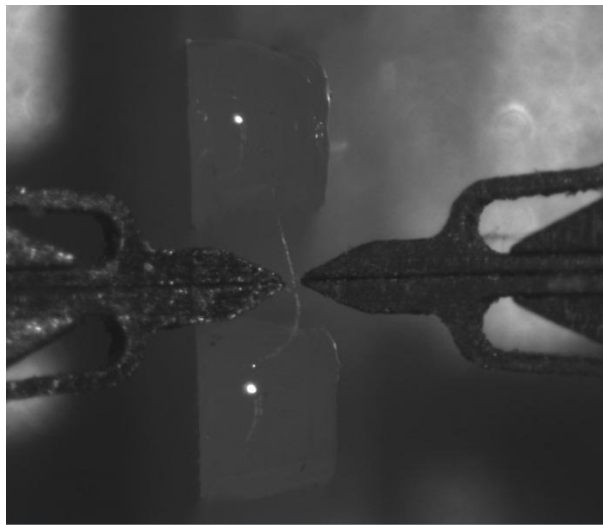


Figure 3.19 - Z-directional force application to IFFB

The output voltage of the PVDF film sensor is converted to force using the calibration curve corresponding to the used velocity. Using the force data acquired from the PVDF force sensor, the force-time curve is obtained for each experiment. A representative result of a Z-Directional IFFB strength measurement is shown in Fig. 3.20.

The ultimate value of the obtained force-time curve is reported as the Z-directional force of the corresponding IFFB. This value is shown in Fig. 3.20 as IFFB breaking point.

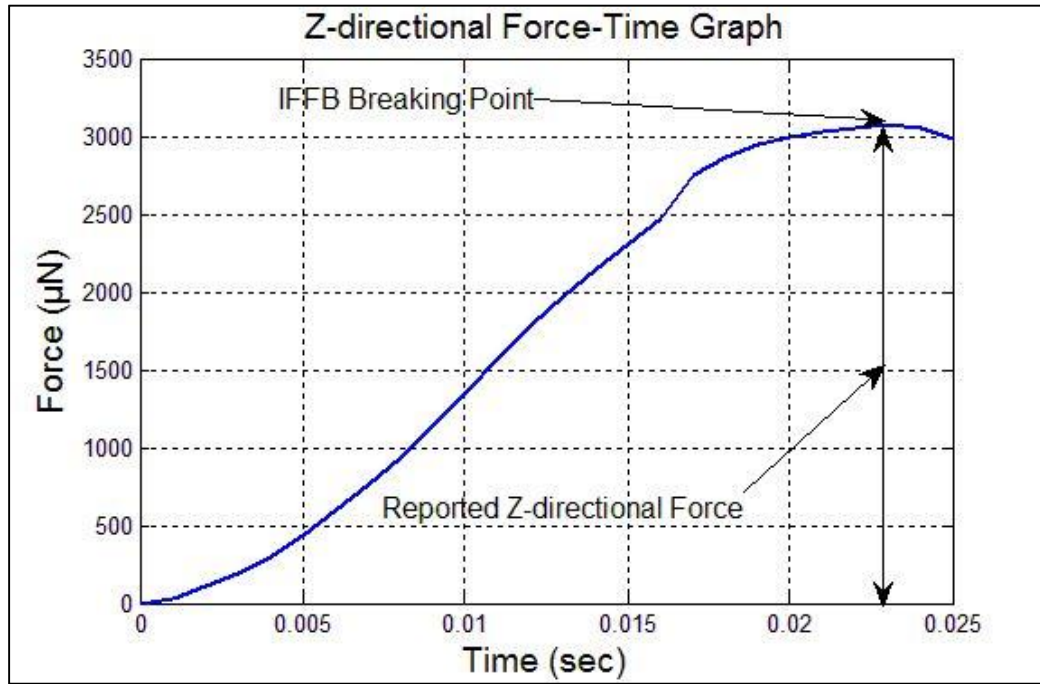


Figure 3.20 - A representative Force-Time curve for the Z-Directional IFFB strength measurement

### 3.3. Microfibril Angle Measurement Method

An experimental method based on the transmission ellipsometry for determining the microfibril angle of individual fibres is developed and integrated to the microrobotic platform. This method is simple, fast, and more accurate than the existing polarized-light methods. Furthermore, no sample pre-treatment is required. The conceptual design, hardware design and implementation, and measurement protocol are described in the next sections.

#### 3.3.1. Conceptual Design

The requirements have been specified for microfibril angle measurement in the first step of design. The first four requirements 1, 2, 3, 4, 7, 8, and 9 in Z-directional IFFB strength measurement are needed for this measurement as well. In addition to those requirements, the following requirements are likewise needed.

1. A polarizer should be positioned under the fibre with  $45^\circ$  angle with the axis of fibre.
2. An analyser should be on top of the fibre (the other side of the fibre).
3. A camera should record the images on top of the analyser.
4. The analyser should be able to rotate from  $0^\circ$  to  $135^\circ$  with respect to the polarizer.

5. The rotation of the analyser should be automated.
6. The resolution of the rotational movement of the analyser should be less than  $2^\circ$ .
7. The light source (illumination) should be under the polarizer.
8. The illumination system should include three different wavelengths preferably blue, green, and red.
9. The change of the light source wavelength should be automated.
10. Image processing software is required for automated analysis of the microfibril angle results. The software should be able to calculate the microfibril angle for all parts of the fibre based on [46].

To address these requirements, a measurement system is conceptually designed. The conceptual design of the measurement system and the main functions are illustrated in Fig. 3.21. The Micromanipulation (F1), Visualization (F2), Sample Storage (F3), and Control (F4) functions have been explained in previous sections. The polarization angle control (F5) and the wavelength control (F6) functions are explained in this section.

Polarization angle control function (F5) enables controlling the angle between the polarizer and analyzer as the angle between polarizer and analyzer should be in certain amounts during the measurement.

Wavelength control function (F2) facilitates changing the wavelength of the light so that the transmission ellipsometry imaging can be performed in different wavelengths.

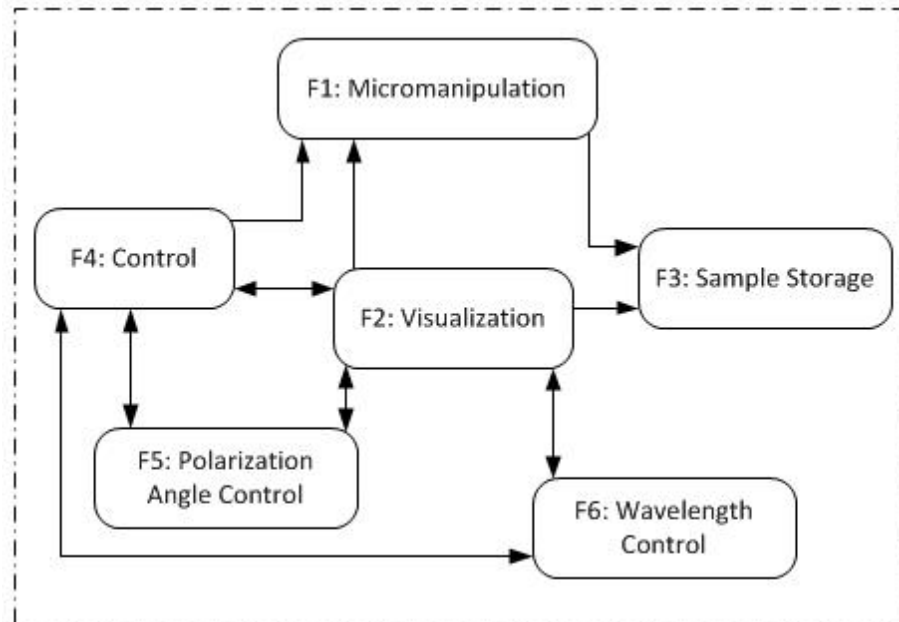


Figure 3.21 - Conceptual design of the method for microfibril angle measurement

The Microrobotic Platform B is used for the experiments since it already includes the micromanipulation, visualization, sample storage, and control functions. The polarization angle control and wavelength control functions should be designed and integrated to the Microrobotic Platform B.

### 3.3.2. Hardware Design and Implementation

Based on the transmission ellipsometry method described in theoretical background of the work, the analyzer attached to the camera optics has to be turned to four different angles,  $0^\circ$ ,  $45^\circ$ ,  $90^\circ$  and  $135^\circ$ , with the polarizer of the light source during the measurements [13]. This feature enables the polarization angle control. In order to automate the measurements, the analyzer has to be motorized. In the original paper [13], the analyzer was adjusted by hand and therefore  $2^\circ$  resolution for the motor is sufficient. In this work, a rotary stepper motor with encoder (Festo, Germany) is connected to the optics of the camera to facilitate the rotation of the analyzer. The motor is connected to the optics with a gear system. The resolution of the motor and the gears together is below  $1^\circ$  which is acceptable in this application. The control unit of the stepper motor is connected to the computer via Ethernet. Festo Configuration Tool (FCT) is used as the control interface of the stepper motor. The final configuration of the motorized analyzer is demonstrated in Fig. 3.22. Since the stepper motor should move gently to minimize the vibration in the whole imaging system, the stepper motor is configured so that the maximum velocity and acceleration of the movement are 2 rpm, and 100 rpm/min, respectively. This guaranties the gentle movement of the stepper motor during MFA measurement procedure.



Figure 3.22 – Motorized analyzer for transmission ellipsometry imaging

The integration of the motorized analyser system to the Microrobotic Platform B is shown schematically in Fig. 3.23.



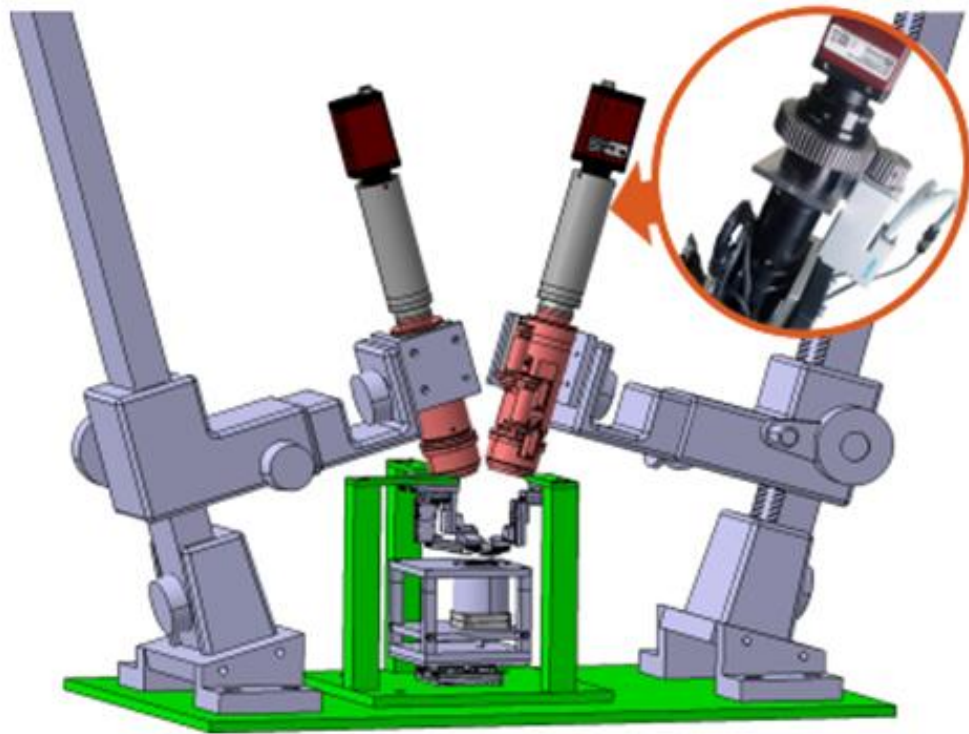


Figure 3.23 – Integration of the motorized analyser to Microrobotic Platform B

For wavelength control of the passing light, the light source of the platform must be capable of multiple wavelength bands to enable the transmission ellipsometry. In the original work [46], different bands between 400nm and 700nm were obtained by applying band pass filters with 80 nm pass bands. Integrating interchangeable band pass filters to the 3-DOF sample stage is problematic and thus the light source of the illumination module is updated to a highflux RGB LED (Edison Opto, Taiwan). The dominant wavelengths of the LED are 465nm, 525nm and 625nm with the approximate bandwidths of 15nm, 40nm and 30nm, respectively. The individual chips of the LED are controlled with a custom-made control circuitry with three 0 – 5V input signals. The light source in three different wavelengths is illustrated in Fig. 3.24.

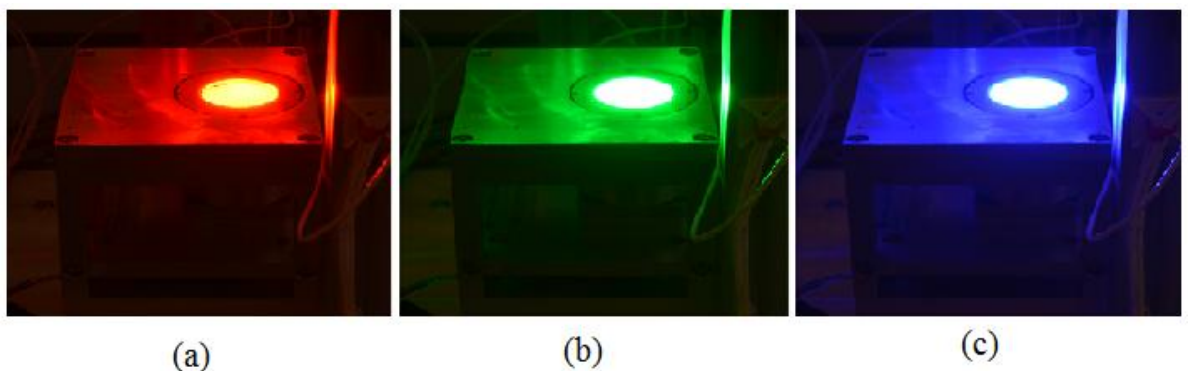


Figure 3.24 – Light source wavelength control – (a) Red light – (b) Green light – (c) blue light



### 3.4. Discussion

In this chapter, a general overview of the microrobotic platforms used in this research work has been given. The Microrobotic Platform A and the Microrobotic Platform B are used for Z-directional IFFB strength measurement and microfibril angle measurement, respectively.

The requirements for Z-directional IFFB strength measurement have been specified and the conceptual design based on requirements has been presented. Since the micromanipulation, visualization, sample storage, and control functions for Z-directional IFFB strength measurement are existed in Microrobotic Platform A, this platform is used for method development and the microforce sensing function is developed and integrated to the platform. As the PVDF microforce response is dependant to the deformation rate of the sensor, the sensor is calibrated for different deformation rates. This facilitates the Z-directional IFFB strength measurement in different deformation rates.

The requirement list and conceptual design for microfibril angle measurement has been given as well. Due to the fact that the micromanipulation, visualization, sample storage, and control functions were existed in Microrobotic Platform B, this platform is used for method development and the polarization angle control and wavelength control functions have been integrated to the platform.

Different experiments have been performed with the developed method to demonstrate their functionality. The results and analysis of the performed experiments are presented in the next chapter.

## 4. Results and Discussion

The research results and their significance are presented in this chapter. This chapter is divided to three parts. In the first part, the results of study on the effect of deformation rate on the PVDF microforce sensor response is presented and discussed. The results of Z-directional fibre-fibre bond strength measurements and related analysis is presented in the second part. The third part includes the results and discussion related to microfibril angle measurement. Possible sources of error are also discussed.

### 4.1. Effect of Deformation Rate on Microforce Sensor Response

As discussed in the previous section, a magnetic encoder is utilized to obtain the average velocity of the piezoelectric microactuator in different actuation frequencies. The average velocity in different actuation frequencies is presented in Table 4.1.

Table 4.1. Average velocity vs. actuation frequency

Actuation frequency (Hz)	1000	2500	5000	7500	10000	12500	15000	17500
Average velocity ( $\mu\text{m/sec}$ )	580	1110	1546	2160	4512	4540	4579	5466

The results are illustrated in terms of the reference sensor force as a function of the output voltage of the PVDF film sensor in Fig. 4.1. For a certain force, the output voltage of the PVDF force sensor decreases when increasing the deformation rate. The calibration curves are slightly different for deformation rates below 2160  $\mu\text{m/sec}$ . However, there is no change in the calibration curve of the sensor for deformation rates more than 2160  $\mu\text{m/sec}$ . In other words, calibration curve stabilizes in deformation rates higher than 2160  $\mu\text{m/sec}$ .

The Eq. 3.1 is used to as the calibration formula to map the output voltage to the Z-directional force for the aforementioned deformation rates. The values of  $P_1$  and  $P_2$  for different deformation rates are illustrated in Table 4.2.

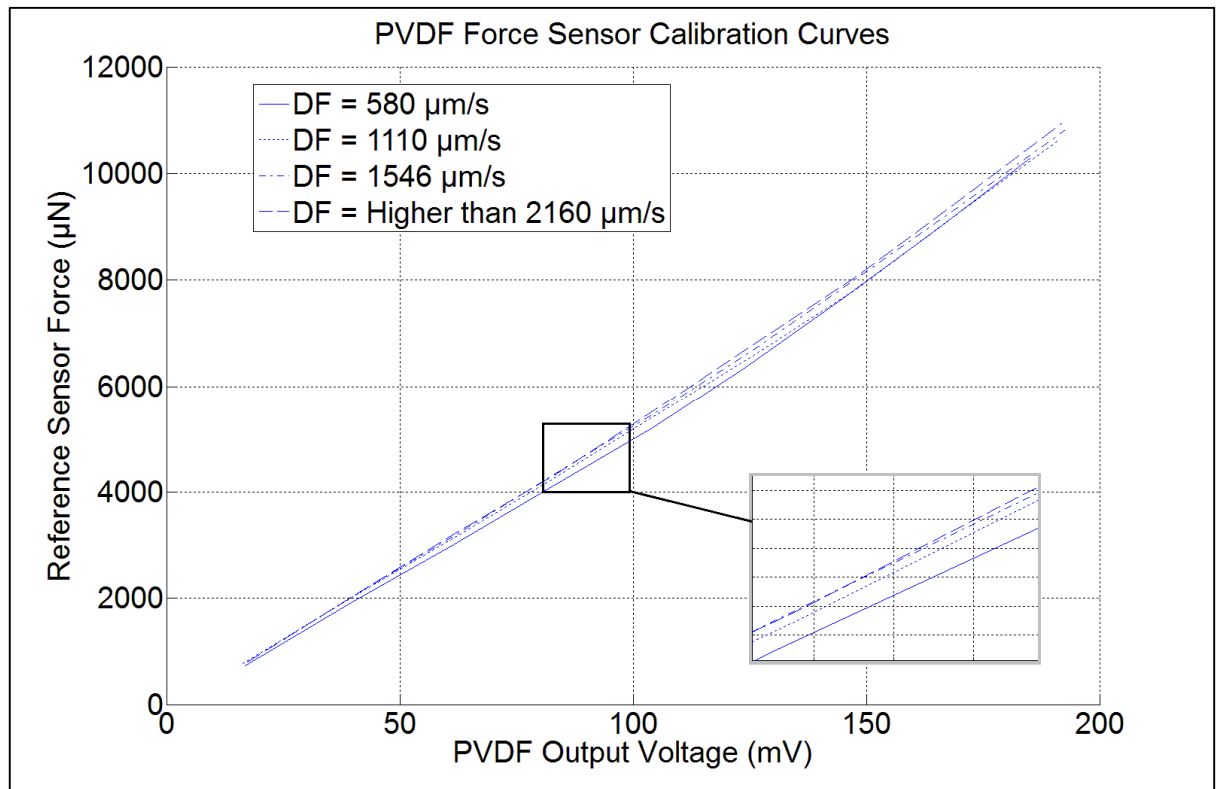


Figure 4.1 - Effect of deformation rate on PVDF force sensor calibration curve.

Table 4.2 - The calibration curves coefficients

Deformation Rate ( $\mu\text{m/sec}$ )	Fitted Line Slope (P1)	Fitted Line Offset (P2)
580	55.81	-285.20
1110	56.25	-417.92
1546	56.81	-315.72
Higher than 2160	58.01	-371.82

In the case that deformation rates between these values are needed to be used in the measurements, two solutions are suggested to utilize in this section.

1. The same calibration experiments should be performed for the test deformation rates if the rate is less than  $2160 \mu\text{m/sec}$ . This would be quite laborious to set the calibration setup for each new deformation rate. However this would be the most accurate solution.
2. The second solution would be accepting the error. In this case the possible range of error should be reported. To make the error calculation process clear, a calculation example is presented. Considering that the deformation rate is  $750 \mu\text{m/sec}$ , and the output voltage of the PVDF sensor is  $200 \text{ mV}$ . If the calibration curve for  $580 \mu\text{m/sec}$  is used, then the force can be calculated as follows.

$$FZ_{580} = 55.81 * 200 - 285.20 = 10876.8 \mu N$$

If the calibration curve for 1110  $\mu m/sec$  is used, then the force can be calculated as follows.

$$FZ_{1110} = 56.25 * 200 - 417.92 = 10832.1 \mu N$$

The reported value for force is the average of two values as follows.

$$FZ_{750} = \frac{FZ_{580} + FZ_{1110}}{2} = 10854.5 \mu N$$

The measurement error can be reported as follows.

$$Error = 10876.8 - 10832.1 = 44.7 \mu N \equiv \pm 22.35 \mu N$$

## 4.2. Z-Directional Fibre-Fibre Bond Strength Measurement Results

As stated in the previous sections, Z-directional fibre-fibre bond strength measurement at the fibre level is facilitated for the first time during this research work. This platform enables multiple studies on this property. For instance, the effect of different paper chemicals on Z-directional bond strength of paper fibres can be investigated. In this thesis work, the effect of refining on bleached softwood Kraft pulp (BSKP) is studied, and the results are interpreted with T-test analysis.

### 4.2.1. The Effect of Refining on Z-Directional Bond Strength

The effect of refining on the strength of papers in handsheet level has been studied already for several decades. The level of refining directly affects the density of the paper which increases the strength of the paper, consequently [41]. Nordman studied the changes in the paper sheets density after refining and how it correlates to the increase of Z-directional tensile strength of paper sheets. However, due to the effect of fibre straining and energy dissipation from the changes in the scattering coefficient, which are included in the final results, his measurements are quite complicated for any comparison [67]. Nanko and Ohsawa studied the mechanisms of fibre bonding and discovered that the more the fibres are beaten; the contact between fibres increases and the bonding layer becomes thicker making the bonds stronger [68]. Gurnagul et al. tried to determine tensile strength of northern softwood Kraft paper sheets using the Page equation. They focused on calculating the effect of refining and drying on the bond strength of a single pulp fibre from paper sheets [69].

While the effect of refining on the paper strength has been studied on the handsheet level, the effect on the fibre level has far less attention and still needs more research. Magnusson et al. studied the differences in the inter-fibre bond strength of different types of pulp with varying degrees of refining and nominal drying pressure. They developed a simple procedure for the specimen preparation of fibre-fibre crosses and tested the shear strength of the fibre bonds depending on the different degree of refining. Through the results they determined that with a larger refining degree, the amount of external fibrils will increase as well resulting in higher bond strength [20].

The experiments have been performed for unrefined bleached softwood Kraft pulp (BSKP) successfully. Five experiments have been performed for the sample. The results of the Z-directional IFFB strength measurements are reported for BSKP in Table 4.3.

Table 4.3 - Z-directional fibre-fibre bond strength of BSKP samples

Test No.	BSKP		
	<i>Z-directional Force (<math>\mu\text{N}</math>)</i>	<i>Visible Overlapping area (<math>\mu\text{m}^2</math>)</i>	<i>Z-Directional IFFB Strength (<math>\text{N}/\text{mm}^2</math>)</i>
1	3394	3046	1.11
2	2279	1827	1.24
3	1803	800	2.25
4	2073	1990	1.04
5	2108	1366	1.54
<i>Mean Value</i>			1.44
<i>Standard Deviation</i>			0.49

The experiments have been performed for refined bleached softwood Kraft pulp (RBSKP) with 100 kWh/t specific refining energy successfully. Five experiments have been performed for the sample. The results of the Z-directional IFFB strength measurements are reported for RBSKP in Table 4.4.

Table 4.4 - Z-directional fibre-fibre bond strength of RBSKP samples

Test No.	RBSKP		
	<i>Z-directional Force (<math>\mu\text{N}</math>)</i>	<i>Visible Overlapping area (<math>\mu\text{m}^2</math>)</i>	<i>Z-Directional IFFB Strength (<math>\text{N}/\text{mm}^2</math>)</i>
1	1951	774	2.52
2	2732	1300	2.10
3	2551	1086	2.35
4	2759	867	3.18
5	3660	1001	3.65
<i>Mean Value</i>			2.76
<i>Standard Deviation</i>			0.64

The summary of the measurements is abstracted in Table 4.5. As can be seen, the refining increases the Z-directional fibre-fibre bond strength of bleached softwood Kraft pulp. The validity of this hypothesis is investigated using T-test analysis in the next section.

Table 4.5 – Summary of the measurements

<b>Sample</b>	<b>Number of Samples</b>	<b>Mean Value</b>	<b>Standard Deviation</b>	<b>Coefficient of Variation</b>
BSKP	5	1.44	0.49	34 %
RBSKP	5	2.76	0.64	23 %

#### 4.2.2. T-Test Analysis of the Results

T-test analysis is used to interpret the results. In the implementation of T-test, BSKP and RBSKP bonds are considered as two groups of samples to investigate if refining affects the Z-directional strength of IFFBs. The two-tailed P value equals to 0.0064. By conventional criteria, this difference is considered to be statistically significant. Hence, based on the performed experiments and unpaired T-test, refining increases the Z-directional strength of bleached softwood Kraft pulp fibre bonds. The summary of T-test analysis results is presented in Table 4.6.

Table 4.6 – Summary of the T-test analysis

<b>Property</b>	<b>t</b>	<b>df</b>	<b>P value</b>	<b>Probability of Null Hypothesis Rejection</b>
Z-directional Fibre-Fibre Bond Strength	3.66	8	0.0063	99.37 %

#### 4.3. Microfibril Angle Measurement - Performance Experiments

Semi-automatic measurement of microfibril angle is facilitated using microrobotics during this thesis work. The microfibril angle measurements have been performed on 11 fibres. Bleached softwood Kraft pulp fibres are used for the experiments. The fibres are placed on top of the glass slide in the sample storage, and the images are taken. Each fibre experiment includes totally eight images for four different analyzer angles (0°, 45°, 90°, and 135°) and two different wavelengths (green and blue light). The images for a sample fibre are shown in Fig. 4.2. The experiments have been performed semi-automatically so that the analyzer angle is changed by the stepper motor software interface, and images have been taken by the computer. The wavelengths have been

changed using the switches of the LED circuit. Imaging the all eight images for each fibre sample takes approximately 20 seconds. In the next step, the images are fed to the MATLAB code for final analysis. The final representation of the result for one sample fibre is shown in Fig. 4.3. Microfibril angle and fibre wall thickness is calculated by the code in every pixel of the fibre image.

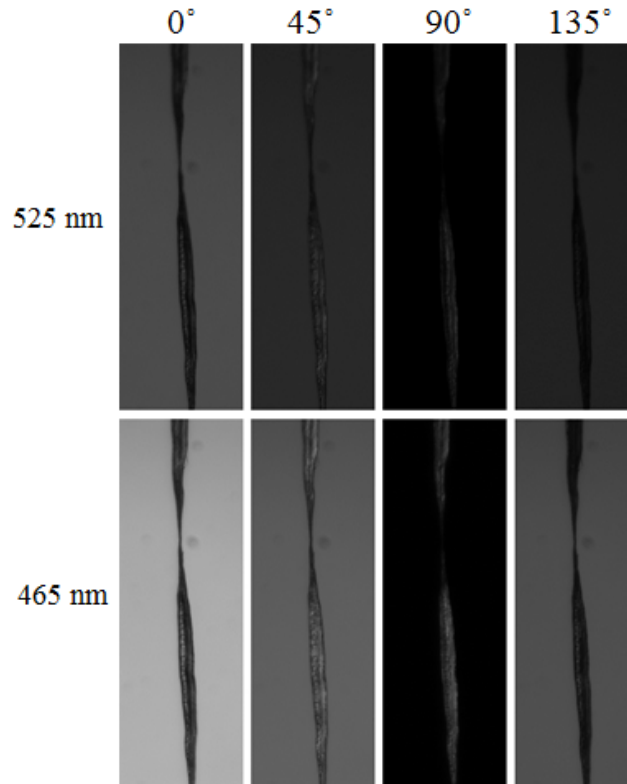


Figure 4.2 – Transmission ellipsometry images of a sample BSKP fibre

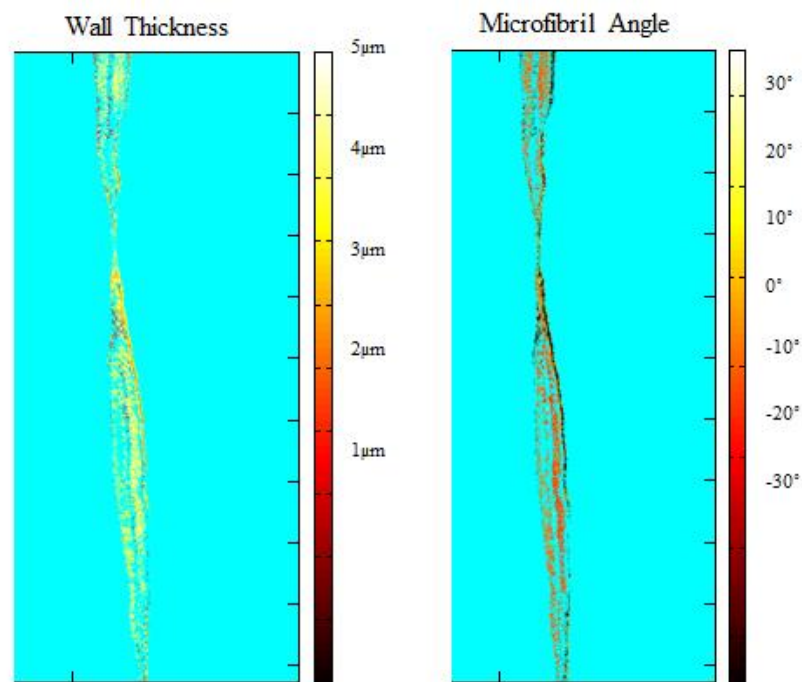


Figure 4.3 – Representation of the microfibril angle measurement

The next set of experiments has been performed on a fibre during stretching to investigate the effect of applying axial tensile stress on the microfibril angle. A bleached softwood Kraft pulp (BSKP) fibre is grasped and straightened using micromanipulators of Microrobotic Platform B (Fig 4.4).



Figure 4.4 – Straightened fibre for microfibril angle measurement

Axial tensile force is applied to the fibre using micromanipulators in eight steps. In each step, the left micromanipulator is moved 5  $\mu\text{m}$  to the left and the needed images for microfibril angle measurement are recorded. The length of the fibre between microgrippers is approximately 2000  $\mu\text{m}$ . Thus, the applied strain can be calculated for each step using as follows.

$$S = \frac{\Delta l}{l_0} \quad (4.1)$$

Where  $S$  is the applied strain,  $\Delta l$  is the fibre length change (micromanipulator displacement), and  $l_0$  is the initial length of the fibre. The applied strain vs. micromanipulator movement is presented in Table 4.7.

Table 4.7 – Applied strain vs. micromanipulator movement

Micromanipulator displacement ( $\mu\text{m}$ )	5	10	15	20	25	30	35	40
Strain	0.0025	0.005	0.0075	0.01	0.0125	0.015	0.0175	0.02

The microfibril angle measurement is performed in all 8 steps. Three zones of the fibre are selected for comparison procedure since the results are more stable and reliable in these three regions. Indeed, the conditions for result validation are met in most of the spots in these zones. The stable zones are marked on the test fibre in Fig. 4.5.



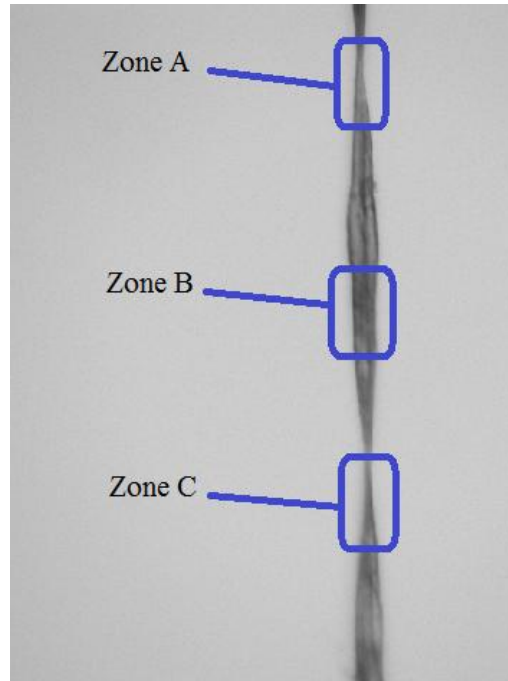


Figure 4.5 – The reliable zones for microfibril angle measurement and comparison

Five rectangular areas are selected in each zone and the average MFA are measured in each rectangular area. The average MFA value of the five measurements in each zone is reported in Table 4.8.

Table 4.8 – Average MFA value in the zones vs. strain

Strain	Average MFA in Zone A	Average MFA in Zone B	Average MFA in Zone C
0	-20.63	0.092	2.004
0.0025	-19.83	0.48	2.5
0.005	-20.43	0.03	2.84
0.0075	-21.266	0.124	2.102
0.01	-23.962	0.642	2.892
0.0125	-24.926	0.238	2.522
0.0150	-23.992	0.076	2.984
0.0175	-25.668	-0.184	2.2
0.02	-26.806	0.532	--- (Not reliable data)

The graphs representing average microfibril angle vs. strain in Zones A, B, and C are illustrated in Figs. 4.6, 4.7, and 4.8, respectively.

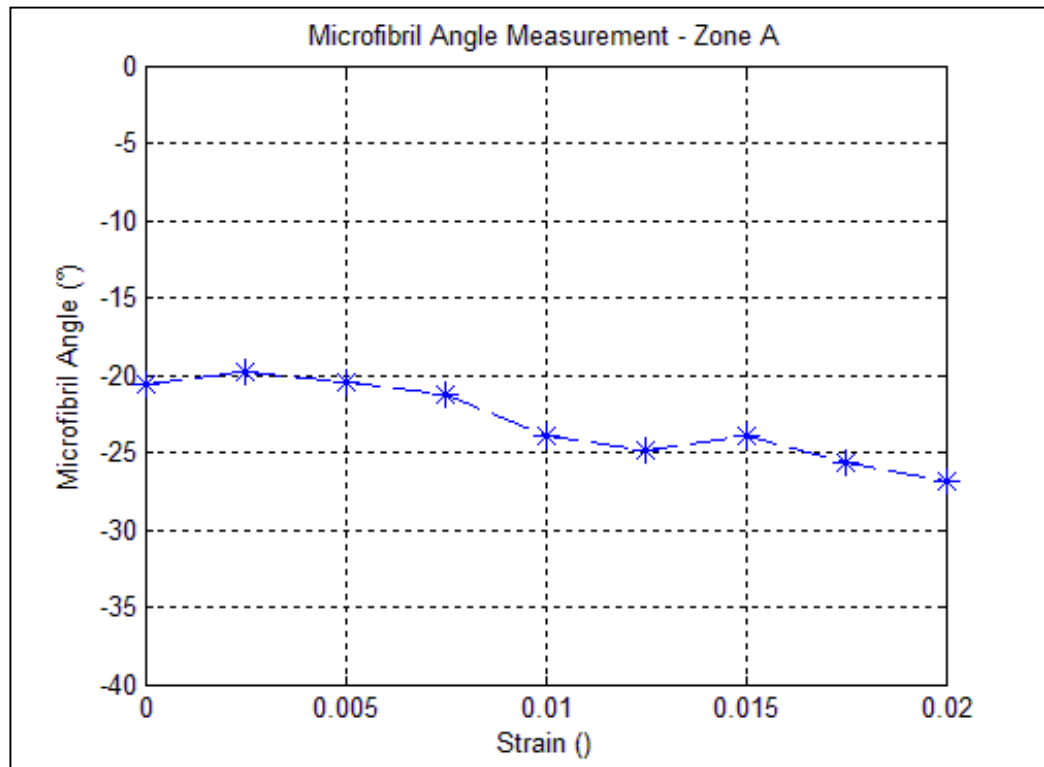


Figure 4.6 – Average microfibril angle vs. strain in Zone A

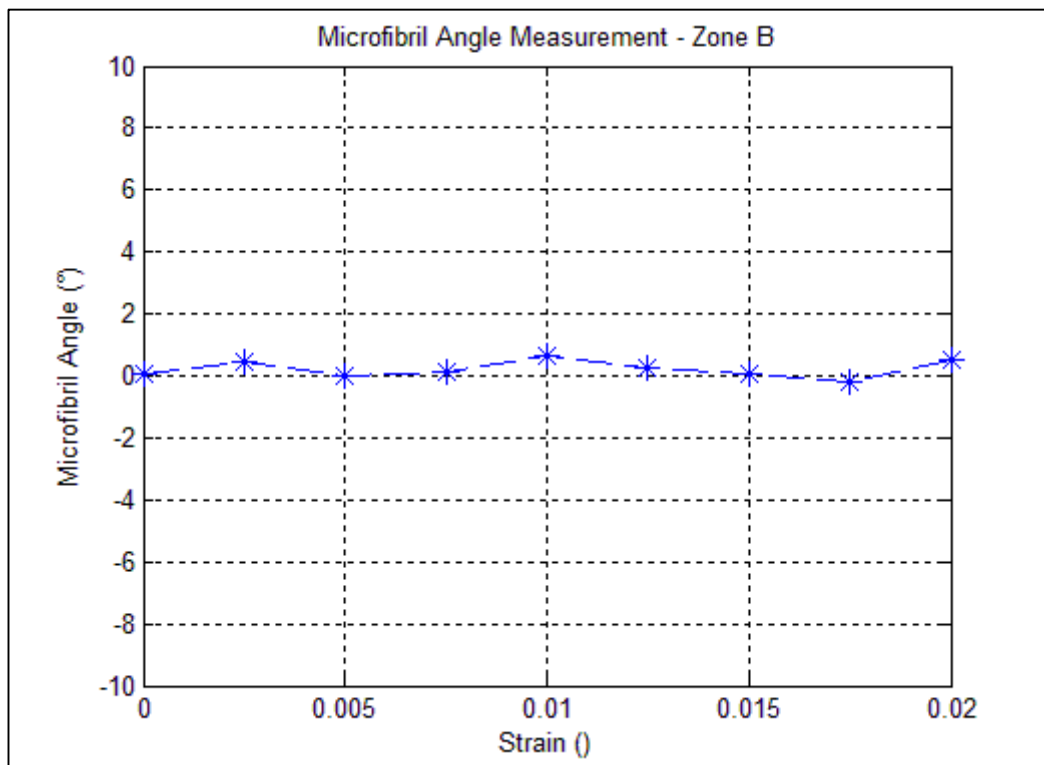


Figure 4.7 – Average microfibril angle vs. strain in Zone B

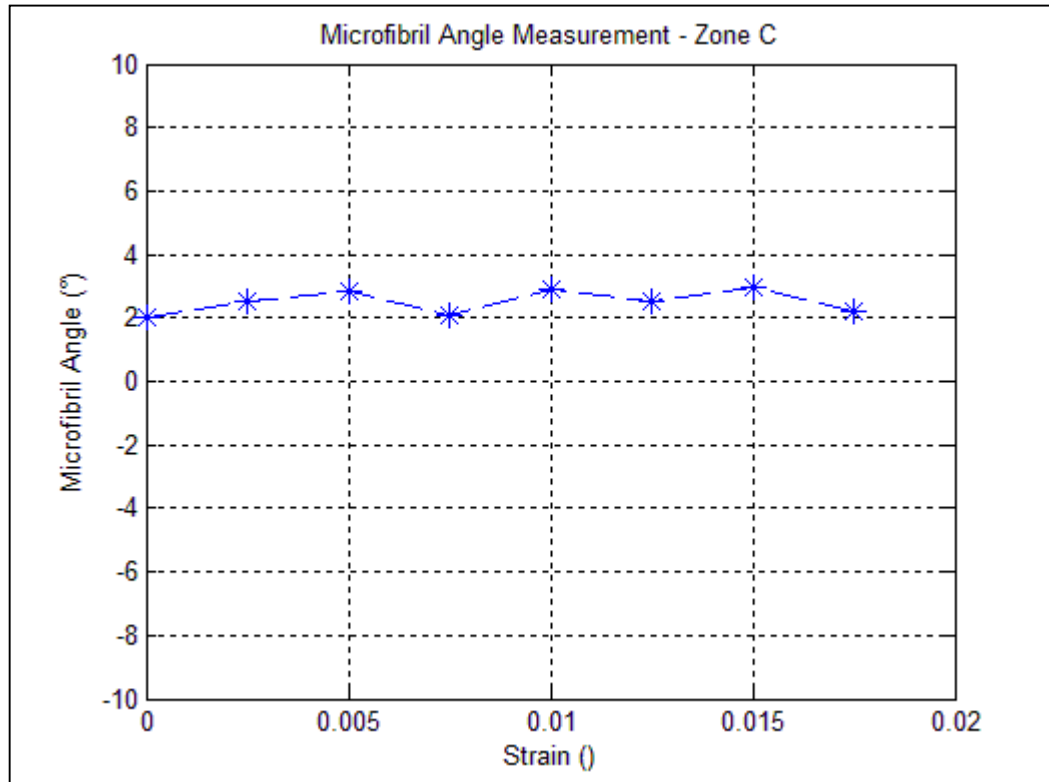


Figure 4.8 – Average microfibril angle vs. strain in Zone C

#### 4.4. Discussion

The PVDF microforce sensor which has been developed in [40] is calibrated for different deformation rates. This facilitates Z-directional IFFB strength measurement for the whole range of deformation rates. It has been demonstrated that the response of the sensor stabilizes after some certain value of the deformation rate. Moreover, a method has been presented to obtain the error in the measurements with deformation rates between the calibrated deformation rate values.

Successful experiments have been performed using the developed Z-directional IFFB strength measurement method. As an application of the system, the effect of refining on Z-directional IFFB strength of BSKP fibres is investigated. The results show that the refining increases the Z-directional IFFB strength of BSKP fibres. In fact, this is a demonstration of the developed method in real needed applications in paper industry. The measurements can be performed to study the effect of other modifications such as adding paper chemicals on the Z-directional IFFB strength.

There are some error sources in the measurements:

- Overlapping area is measured by visual inspection which is not necessarily equal to the actual bonded area.

- The overlapping area is measured from top view. Thus, the projection of the visible overlapping area is measured which is a portion of the total visible overlapping area.
- Other modes of loading such as shear and torsion modes can be coupled to the results due to non-idealities in force application and IFFB mounting.

The experiments have been done using the developed microfibril angle measurement method to demonstrate the performance of the system. Two sets of measurements have been performed. In the first measurement set, the MFA of individual fibres placed on the sample holder freely (no grasping) are measured. There were no reference measurements of the MFA of the fibre samples measured available; however, a senior fibre scientist described the data convincing and the system promising.

In the second measurements set, the MFA of an individual fibre while applying axial tensile stress is measured. The stress is applied using the micromanipulators. The graphs showing average MFA in different zones of fibre vs. strain have been drawn. It would be difficult to conclude any hypothesis related to the effect of strain on the microfibril angle based on these measurements. However, it has been demonstrated that the developed system is capable of simultaneous measurement of MFA and mechanical properties such as strain. Moreover, the MFA measurement can be performed during single fibre manipulation.

## 5. Conclusions

This thesis work introduces a novel method for the experimental evaluation of the Z-directional bond strength using microrobotics and a Polyvinylidene fluoride (PVDF) film microforce sensor which facilitates measuring Z-directional bond strength at the single fibre level for the first time. Besides, an experimental method based on microscopic transmission ellipsometry for semiautomatic measurement of microfibril angle at fibre level is also developed. Indeed, this is the first system which enables simultaneous measurement of Z-directional bond strength and microfibril angle at the individual fibre level is developed during this research work.

The PVDF microforce sensor is calibrated for different deformation rates. Resulted calibration curves demonstrate little difference in the output voltage of the PVDF force sensor for deformation rates below 2160  $\mu\text{m}/\text{sec}$  i.e. 7500 Hz actuation frequency; however, calibration curve stabilizes in deformation rates higher than 2160  $\mu\text{m}/\text{sec}$ .

Some aspects of the Z-directional IFFB measurement method makes it advantageous in comparison with other methods of bond strength measurement. Since the force is applied in Z-direction of the IFFB, this method takes the mode of loading into account. Since there is a high potential for automation in microrobotics –which is used as a tool in this study-, some functions in this measurement method has the capability of being performed automated and high throughput in the future. Automation studies are an ongoing research on the utilized microrobotic platform. Moreover, using microrobotics decreases the human interaction with the IFFBs. However, there are some error sources in the measurements. Overlapping area is measured by visual inspection which is not necessarily equal to the actual bonded area. Other modes of loading such as shear and torsion modes can be coupled to the results due to non-idealities in force application and IFFB mounting.

This measurement method enables multiple studies on Z-directional bond strength. The effect of different paper chemicals on Z-directional bond strength of paper fibres can be investigated. In this thesis work, the effect of refining on the Z-directional strength of bleached softwood Kraft pulp fibre bonds has been investigated. Unrefined and refined bleached softwood Kraft pulp fibres are used for the experiments. Unpaired T-test is used to analyse the results. The results indicate that refining increases the Z-directional strength of bleached softwood Kraft pulp fibre bonds.

Furthermore, a semi-automatic system for experimental evaluation of microfibril angle at the individual fibre level is developed and integrated to the microrobotic platform for fibre studies. We integrated the components needed for the measurements to the platform. The operation of the system by semi-automatic measurement of the MFA from 10 fibres placed on the sample stage and one fibre that was grasped is demonstrated. However, the design enables automatic measurements. Measurement of the Microfibril angle can be performed while doing fibre manipulation, fibre tensile test or flexibility measurement. Moreover, sample pre-treatment is not needed in this method.

The feasibility of Z-directional individual fibre-fibre bond strength measurement has been demonstrated during this thesis work. Future work includes development of the components for semi or fully automated Z-directional individual fibre-fibre bond strength measurement. Towards this goal, increasing the level of autonomy in microrobotics by means of intelligence methods is indisputably a building block. Moreover, fully automated microfibril angle measurement can also be seen as a future work which can be achieved with a little effort. From the paper physics prospective, hundreds of Z-directional bond strength experiments can be performed to provide sufficient amount of data such that realistic strength distributions of wood fibre bonds can be incorporated into fibre network models. This will provide new knowledge on papermaking fibres. Investigation on the effect of paper chemicals on Z-directional bond strength and microfibril angle can also be done with the developed methods.

## REFERENCES

- [1] M. F. Pantano, H. D. Espinosa and P. Leonardo, "Mechanical characterization of materials at small length scales," *Journal of Mechanical Science and Technology*, vol. 26, no. 2, pp. 545-561, 2012.
- [2] Y. Bellouard, *Microrobotics: methods and applications*, CRC, 2010.
- [3] N. Chaillet and S. Regnier, *Microrobotics for Micromanipulation*, Wiley, 2010.
- [4] J. Cecil, D. Powell and D. Vasquez, "Assembly and manipulation of micro devices—A state of the art survey," *Robotics and Computer-Integrated Manufacturing*, vol. 23, no. 5, p. 580–588, 2007.
- [5] S. Fatikow, S. Jörg, A. Buerkle and F. Schmoeckel, "A flexible microrobot-based microassembly station," *Journal of Intelligent and Robotic Systems*, vol. 27, no. 1-2, pp. 135-169, 2000.
- [6] D. O. Popa and E. S. Harry, "Micro and mesoscale robotic assembly," *Journal of manufacturing processes*, vol. 6, no. 1, pp. 52-71, 2004.
- [7] V. K. Asari, K. Sanjiv and M. K. Irwan, "A fully autonomous microrobotic endoscopy system," *Journal of Intelligent and Robotic Systems*, vol. 28, no. 4, pp. 325-341, 2000.
- [8] K. Pahlavan, Y. Ye, U. Khan and R. Fu, "RF localization inside human body: Enabling micro-robotic navigation for medical applications," in *International Conference on Localization and GNSS (ICL-GNSS)*, Tampere, 2011.
- [9] J. P. Desai, A. Pillarisetti and A. D. Brooks, "Engineering approaches to biomanipulation," *Annual Review of Biomedical Engineering*, vol. 9, no. 1, pp. 35-53, 2007.
- [10] H. Matsuoka, T. Komazaki, Y. Mukai, M. Shibusawa, H. Akane, A. Chaki, N. Uetakec and M. Saito, "High throughput easy microinjection with a single-cell manipulation supporting robot," *Journal of biotechnology*, vol. 116, no. 2, pp. 185-194, 2005.
- [11] Y. Sun and B. J. Nelson, "Biological cell injection using an autonomous microrobotic system," *The International Journal of Robotics Research*, vol. 21, no. 10-11, pp. 861-868, 2002.
- [12] C. Ververis, K. Georgiou, N. Christodoulakis, P. Santas and R. Santas, "Fiber dimensions, lignin and cellulose content of various plant materials and their suitability for paper production," *Industrial Crops and Products*, vol. 19, no. 3, p. 245–254, 2004.
- [13] P. Saketi, A. Treimanis, P. Fardim, P. Ronkanen and P. Kallio, "Microrobotic platform for manipulation and flexibility measurement of individual paper fibers," in *IEEE/RSJ International Conference on Intelligent Robots and Systems (IROS)*,

Taipei, 2010.

- [14] P. Saketi and P. Kallio, "Microrobotic platform for making, manipulating and breaking individual paper fiber bonds," in *IEEE International Symposium on Assembly and Manufacturing (ISAM)*, Tampere, 2011.
- [15] P. Saketi, M. Mikczinski, S. Fatikow and P. Kallio, "Investigation of Aged Fibre-fibre Bonds with Micro and Nanorobotic Tools," in *Proceedings of 15th Pulp and Paper Fundamental Research Symposium*, Cambridge, 2013.
- [16] P. Saketi and P. Kallio, "Measuring Bond Strength of Individual Paper Fibers using Microrobotics," in *Progress in Paper Physics*, Graz, 2011.
- [17] P. Saketi, J. Hirvonen, Y. Lai, C. Ganser, C. Teichert, J. Jarnstrom, P. Fardim and P. Kallio, "Automated Drop-on-Fiber contact angle measurement using a microrobotic platform," *NORDIC PULP & PAPER RESEARCH JOURNAL*, vol. 29, no. 2, pp. 225-231, 2014.
- [18] R. J. Dinus and T. Welt, "Tailoring fibre properties to paper manufacture: Recent developments," *Tappi Journal*, vol. 80, pp. 127-139, 1997.
- [19] W. J. Fischer, U. Hirn, W. Bauer and R. Schennach, "Testing of individual fibre-fibre joints under biaxial load and simultaneous analysis of deformation," *Nordic Pulp and Paper Research Journal*, vol. 27, pp. 237-244, 2012.
- [20] M. S. Magnusson, X. Zhang and S. Östlund, "Experimental Evaluation of the Interfibre Joint Strength of Papermaking Fibres in Terms of Manufacturing Parameters and in Two Different Loading Directions," *Experimental Mechanics*, vol. 53, pp. 1621-1634, 2013.
- [21] K. Joshi, K. Batchelor and K. A. Rasid, "Investigation of the effect of drying and refining on the fibre-fibre shear bond strength measured using tensile fracture line analysis of sheets weakened by acid gas exposure," *Cellulose*, vol. 18, no. , pp. 1407-1421, 2011.
- [22] S. Reyier, O. Ferritsius and O. Shagaev, "Measuring the debonding ability distribution of fibres in mechanical pulps," *Tappi Journal*, pp. 26-32, 2008.
- [23] T. Fukuda, F. Arai and M. Nakajima, *Micro-Nanorobotic Manipulation Systems and Their Applications*, Springer, 2013.
- [24] R. A. Speers, T. D. Durance, M. A. Tung and J. Tou, "Colloidal properties of flocculent and nonflocculent brewing yeast suspensions," *Biotechnology progress*, vol. 9, no. 3, pp. 267-272, 1993..
- [25] Z. Lu, P. C. Chen and W. Lin, "Force sensing and control in micromanipulation," *IEEE Transactions on Systems, Man, and Cybernetics, Part C: Applications and Reviews*, vol. 36, no. 6, pp. 713-724, 2006.
- [26] T. Tanikawa, M. Kawai, N. Koyachi, T. Arai, T. Ide, S. Kaneko, R. Ohta and T. Hirose, "Force control system for autonomous micro-manipulation," in *IEEE International Conference on Robotics and Automation (ICRA)*, 2001.



- [27] A. Menciassi, A. Eisinger, M. C. Carrozza and P. Dario, "Force sensing microinstrument for measuring tissue properties and pulse in microsurgery," *IEEE/ASME Transactions on Mechatronics*, vol. 8, no. 1, pp. 10-17, 2003..
- [28] F. Arai, A. Kawaji, T. Sugiyama, Y. Onomura, M. Ogawa, T. Fukuda, H. Iwata and K. Itoigawa, "3D micromanipulation system under microscope," in *International Symposium on Micromechatronics and Human Science*, 1998.
- [29] D. H. Kim, B. Kim and H. Kang, "Development of a piezoelectric polymer-based sensorized microgripper for microassembly and micromanipulation," *Microsystem technologies*, vol. 10, no. 4, pp. 275-280, 2004.
- [30] D. H. Kim, Y. Sun, S. Yun, S. H. Lee and B. Kim, "Investigating chorion softening of zebrafish embryos with a microrobotic force sensing system," *Journal of biomechanics*, vol. 38, no. 6, pp. 1359-1363, 2005.
- [31] Y. Shen, N. Xi, W. J. Li and J. Tan, "A high sensitivity force sensor for microassembly: design and experiments," in *IEEE/ASME International Conference on Advanced Intelligent Mechatronics*, Shen, Y., Xi, N., Li, W. J., & Tan, J. (2003, July). A high sensitivity force sensor for microassembly: design and experiments. In *Advanced Intelligent Mechatronics, 2003. AIM 2003. Proceedings. 2003 IEEE/ASME International Conference on* (Vol. 2, pp. 703-, 2003).
- [32] C. K. Fung, I. Elhajj, W. J. Li and N. Xi, "A 2-D PVDF force sensing system for micro-manipulation and micro-assembly," in *IEEE International Conference on Robotics and Automation (ICRA)*, 2002.
- [33] S. Fahlbusch and S. Fatikow, "Force sensing in microrobotic systems-an overview," in *IEEE International Conference on Electronics, Circuits and Systems*, 1998.
- [34] Y. Sun, K. T. Wan, K. P. Roberts, J. C. Bischof and B. J. Nelson, "Mechanical property characterization of mouse zona pellucida," *IEEE Transactions on NanoBioscience*, vol. 2, no. 4, pp. 279-286, 2003.
- [35] A. A. G. Requicha, S. Meltzer, F. T. Arce, J. H. Makaliwe, H. Sikén, S. Hsieh and M. E. Thompson, "Manipulation of nanoscale components with the AFM: principles and applications," in *IEEE Conference on Nanotechnology (IEEE-NANO)*, 2001.
- [36] X. Tian, N. Jiao, L. Liu, Y. Wang, N. Xi, W. Li and Z. Dong, "An AFM based nanomanipulation system with 3D nano forces feedback," in *International Conference on Intelligent Mechatronics and Automation*, 2004.
- [37] H. Sixta, *Handbook of Pulp*, WILEY-VCH, 2006.
- [38] F. J. Schmied, C. Ganser, W. Fischer, U. Hirn, W. Bauer, R. Schennach and C. Tiecher, "Insights into single fibre-fibre bonds using atomic force microscopy," in *Progress in Paper Physics*, Graz, 2011.
- [39] D. H. Page and M. Macleod, "Fibre strength and its impact on tear strength," *Tappi*

*Journal*, pp. 172-174, 1992.

- [40] P. Saketi, S. K. Latifi, J. Hirvonen, S. Rajala, A. Vehkaoja, T. Salpavaara, J. Leikkala and P. Kallio, "Bending PVDF film microforce sensor for Z-directional strength measurement of paper fibre bonds," *Sensors and Actuators A: Physical*, Unpublished.
- [41] A. Koubaa and Z. Koran, "Measure of the internal bond strength of paper/board," *Tappi Journal*, vol. 78, pp. 103-111, 1995.
- [42] J. M. Considine, D. W. Vahey, R. Gleisner, A. Rudie, S. R. Roscoat and J. F. Bloch, "Z-direction fibre orientation in paperboard," *Tappi Journal*, pp. 25-32, 2010.
- [43] C. Fellers, S. Östlund and P. Mäkelä, "Evaluation of the Scott bond test method," *Nordic Pulp and Paper Research Journal*, vol. 27, pp. 231-236, 2012 .
- [44] A. F. Button, "Fiber-fiber bond strength: A study on the linear elastic model structure," Institute of Paper Chemistry, 1979.
- [45] R. A. Stratton and N. L. Colson, "Dependence of fiber/fiber bonding on some papermaking variables," In MRS Proceedings, Cambridge University Press., 1990.
- [46] C. Ye and O. Sundstrom, "Determination of S2-fibril-angle and fiber-wall thickness by microscopic transmission ellipsometry," *Tappi journal*, vol. 80, no. 6, pp. 181-190, 1997.
- [47] K. Niskanen, Book 16: Paper Physics, Helsinki: Fapet Oy, 1998.
- [48] R. D. Preston, "The organization of the cell wall of the conifer tracheid," *Philosophical Transactions of the Royal Society of London. Series B, Biological Sciences*, vol. 224, no. 511, pp. 131-174, 1934.
- [49] D. H. Page, "A method for determining the fibrillar angle in wood tracheids," *Journal of Microscopy*, vol. 90, no. 2, pp. 137-143, 1969.
- [50] L. A. Donaldson, "The use of pit apertures as windows to measure microfibril angle in chemical pulp fibers," *Wood and Fiber Science*, vol. 23, no. 2, pp. 290-295, 1991.
- [51] J. P. Verbelen and D. Stickens, "In vivo determination of fibril orientation in plant cell walls with polarization CSLM," *Journal of Microscopy*, vol. 177, no. 1, pp. 1-6, 1995.
- [52] W. Batchelor, I. H. Parker and A. B. Conn, Measuring the fibril angle of fibres using confocal microscopy, CRC Publications Committee, 1997.
- [53] H. Abe, J. Ohtani and K. Fukazawa, "FE-SEM observations on the microfibrillar orientation in the secondary wall of tracheids," *IAWA Bull*, vol. 12, p. 431-438, 1991.
- [54] R. O. Marts, "Fluorescence microscopy for measuring fibril angles in pine tracheids," *Biotechnic & Histochemistry*, vol. 30, no. 5, pp. 243-248, 1955.
- [55] S. Pleasants, W. J. Batchelor and I. H. Parker, Measuring the fibril angle of

- bleached fibres using micro-Raman spectroscopy, CRC Publications Committee., 1998.
- [56] L. Donaldson and A. Frankland, "Ultrastructure of iodine treated wood," *Holzforschung*, vol. 58, no. 3, pp. 219-225, 2004.
  - [57] D. Reis and B. Vian, "Helicoidal pattern in secondary cell walls and possible role of xylans in their construction," *Comptes rendus biologiques*, vol. 327, no. 9, pp. 785-790, 2004.
  - [58] L. Donaldson and P. Xu, "Microfibril orientation across the secondary cell wall of Radiata pine tracheids," *Trees*, vol. 19, no. 6, pp. 644-653, 2005.
  - [59] H. H. Wang, J. G. Drummond, S. M. Reath, K. Hunt and P. A. Watson, "An improved fibril angle measurement method for wood fibres," *Wood Science and Technology*, vol. 34, no. 6, pp. 493-503, 2001.
  - [60] I. D. Cave, "Theory of X-ray measurement of microfibril angle in wood," *Wood Science and Technology*, vol. 31, no. 4, pp. 225-234, 1997.
  - [61] U. Sahlberg, L. Salmén and A. Oscarsson, "The fibrillar orientation in the S2-layer of wood fibres as determined by X-ray diffraction analysis," *Wood science and technology*, vol. 31, no. 2, pp. 77-86, 1997.
  - [62] L. Schimleck, R. Evans and J. Ilic, "Application of near infrared spectroscopy to a diverse range of species demonstrating wide density and stiffness variation," *IAWA journal*, vol. 22, no. 4, pp. 415-429, 2001.
  - [63] C. Ye, M. O. Sundström and K. Remes, "Microscopic transmission ellipsometry: measurement of the fibril angle and the relative phase retardation of single, intact wood pulp fibers," *Applied optics*, vol. 33, no. 28, pp. 6626-6637, 1994.
  - [64] P. Saketi, M. Von Essen, M. Mikeczinski, S. Heinemann, S. Fatikow and P. Kallio, "A flexible microrobotic platform for handling microscale specimens of fibrous materials for microscopic studies," *Journal of microscopy*, vol. 248, no. 2, pp. 163-171, 2012.
  - [65] J. Hirvonen, A. Hanninen and P. Kallio, "Design and implementation of an illumination system for microrobotic paper fiber studies," in *IEEE International Conference on Robotics and Automation (ICRA)*, 2014.
  - [66] M. von Essen, J. Hirvonen, S. Kuikka and P. Kallio, "Robotic software frameworks and software component models in the development of automated handling of individual natural fibers," *Journal of Micro-Bio Robotics*, vol. 9, no. 1-2, pp. 29-45, 2014..
  - [67] L. S. Nordman, "Bonding in paper sheets: Fundamentals of papermaking fibers.," *British Pulp and Paper Manufacturing Ass., Kenley*, p. 333-347, 1958.
  - [68] H. Nanko and J. Ohsawa, "Mechanisms of fibre bond formation," in *Transactions of the 9th Fundamental Research Symposium on Fundamentals of Papermaking*, 1989.

- [69] N. Gurnagul, S. Ju and D. H. Page, "Fibre-fibre bond strength of once dried pulps," *Journal of Pulp and Paper*, pp. 88-91, 2001.
- [70] L. Leney, "A technique for measuring fibril angle using polarized light," *Wood and Fiber Science*, vol. 13, no. 1, pp. 13-16, 1981.
- [71] D. H. Page, "A method for determining the fibrillar angle in wood tracheids," *Journal of Microscopy*, vol. 90, no. 2, pp. 137-143, 1969.